Jurnal Sylva Lestari

Full Length Research Article

Physical and Mechanical Properties of Cross-Laminated Timber Made of a Combination of Mangium-Puspa Wood and Polyurethane Adhesive

Tengku Muhammad Renzy Hariz[1], Yusuf Sudo Hadi[1,*], Muhammad Adly Rahandi Lubis[2,**], Muhammad Iqbal Maulana[2], Rita Kartika Sari[1], Wahyu Hidayat[3]

[1] Department of Forest Products, Faculty of Forestry and Environment, IPB University. Jl. Ulin, Kampus IPB Darmaga Bogor, 16680, Bogor, Indonesia
[2] Research Center for Biomass and Bioproducts, National Research and Innovation Agency (BRIN). Jl. Raya Jakarta-Bogor Km. 46, Cibinong, Bogor, 16911, Indonesia
[3] Department of Forestry, Faculty of Agriculture, University of Lampung. Jl. Sumantri Brojonegoro 1, Bandar Lampung, 35145, Indonesia
* Corresponding Author. E-mail address: yshadi@indo.net.id
**Corresponding Author. E-mail address: marl@biomaterial.lipi.go.id

ABSTRACT

This study aimed to evaluate the physical and mechanical properties of cross-laminated timber (CLT) characteristics from mangium (*Acacia mangium*) and puspa (*Schima wallichii*) woods and their combination using polyurethane (PU 1.2) adhesives. The manufacture of CLT began with basic adhesive characterization and thermo-mechanical analysis. Wood material's physical and chemical properties were also tested with its response to the PU 1.2 wettability. The CLT $(100 \times 30 \times 3.60)$ cm^3 was manufactured with 160 g/m^2 glue spread at a pressure of 0.80 MPa for 200 minutes. The CLT panels were characterized refers to the JAS 3079 standard. The results show that PU 1.2 had a gelatination time of 182.1 minutes at 25°C, was able to form urethane groups, and experienced an increase in storage modulus at 35°C. Mangium and puspa woods have different physical and chemical properties, but they interact similarly with PU 1.2 wettability. Puspa CLT panel has a higher density than mangium but lower dimensional stability. The bending mechanical properties of hybrid puspa-mangium-puspa CLT were able to match puspa CLT and have one sample of shear strength that met the JAS 3079 standard in both grain directions. Therefore, hybrid puspa-mangium-puspa CLT has the potential to be developed to improve its dimensional stability and mechanical properties.

1. Introduction

Timber can be utilized as a structural construction material that is strong and harmless to the ecosystem. Substituting conventional construction materials with timber at the urban building scale can reduce CO₂ emissions (Amiri et al. 2020; Himes and Busby 2020; Nepal et al. 2016; Pajchrowski et al. 2014). In addition, wood panels also have a higher strength-to-weight proportion than steel (Wimmers 2017). This encourages using wood panels such as Cross-Laminated Timber (CLT). Globally, CLT production in 2020 will reach 2.8 million m^3, potentially increasing production capacity to 4 million m^3 by 2025 (UNECE 2021). The development of CLT accompanied the increase in production as a multi-storey construction material that is resistant to

earthquakes (Follesa et al. 2013; Hummel and Seim 2019; Trutalli and Pozza 2018), fire (Aristri et al. 2021; Schmid 2019) and has high dimensional flexibility (Kuilen et al. 2011). In addition, applying CLT in buildings can be economically advantageous due to the fast and easy construction process (Karacebeyli and Douglas 2013) and efficient circular economic practices (Neykov et al. 2020). However, CLT applications tend to be limited to softwood species as raw materials (Aicher et al. 2016; Marko et al. 2016; Wang et al. 2017; Zhou et al. 2020). Another disadvantage of CLT is that it requires many raw materials (Mallo dan Espinoza 2014), so it is fundamental to utilize hardwood with high production.

Mangium (*Acacia mangium*) can be the choice of hardwood species for CLT. Mangium is a wood species with the highest production in Indonesia in 2020 at 32 million m^3 (Statistics Indonesia 2021). The use of mangium as a 3-layer CLT has been investigated using synthetic adhesives (Yusof et al. 2019a). However, the shear strength of the mangium CLT did not meet commercial mechanical standards (Yusof et al. 2019b). The mechanical properties of CLT can be increased by combining two types of raw materials (Corpataux et al. 2020). One of the other hardwood species that has the potential as a combination for mangium CLT is puspa (*Schima wallichii*). Puspa wood from plantation forests has a specific gravity ranging from 0.57 to 0.61 (Hadjib et al. 2010). This value has met the requirements for the specific gravity of CLT raw materials of 0.35 (American National Standards Institute 2018). In addition, puspa wood has been shown to be a temporary housing material resistant to earthquakes (Ghimire et al. 2020). However, the use of puspa as CLT and its combination with mangium has not been reported.

Differences in the basic properties of the wood used can affect the quality of inter-lamina bonding in CLT (Adnan et al. 2021; Yusoh et al. 2021). Generally, wood species' effect on CLT significantly correlates to the quality of the adhesive used (Hovanec 2015). One type of adhesive that is compatible with CLT is polyurethane (PU). The application of PU-based adhesives to CLT resulted in a lower delamination percentage than CLT with epoxy and phenol resorcinol formaldehyde adhesives, as well as better mechanical properties than CLT with emulsion polymer isocyanate, epoxy, and phenol resorcinol formaldehyde adhesives (Aisyah et al. 2021; Baskara et al. 2022; Hariz et al. 2021; Zelinka et al. 2019). In addition, PU is also indicated to be low in emissions in its use as an exterior adhesive (Liang et al. 2021). Although the quality of mangium CLT using PU adhesives does not meet commercial shear mechanical standards (Yusof et al. 2019b), the adhesion of PU can be further developed by increasing the isocyanate-polyol ratio (Nacas et al. 2017). Therefore, exploring the PU properties of a few sorts of wood as CLT material is significant. Overall, this research aimed to evaluate the CLT characteristics of mangium, puspa, and their combination using PU adhesives.

2. Materials and Methods

Seven-year-old mangium heartwood with a diameter of 25 cm and thirty-year-old puspa wood with a diameter of 32 cm were harvested from Gunung Walat University Forest, Sukabumi, West Java, Indonesia. The polyurethane adhesive used is a two-component PU adhesive from the reaction of isocyanate and polyol obtained from PT. Anugerah Raya Kencana, Serpong, Banten, Indonesia. PU adhesives were prepared with an isocyanate-polyol molar ratio, according to Kong et al. (2011), which is 1.2.

2.1. Characterization of PU 1.2

The characterization of PU 1.2 adhesive was carried out through several parameters, including solids content, gelatination time, viscosity, functional group, chemical compound, and thermo-mechanical analysis (Gurunathan et al. 2015).

2.1.1. Solid content (SC)

The testing sample of 1.5 g PU 1.2 on aluminium foil (Alumunium-foil, Klinpak, Indonesia) was placed in an oven (Memmert celsius 10.0, Memmert, Germany) at a temperature of $105 \pm 2°C$ for 3 h so that the liquid substances in the adhesive reduced to a constant and then weighed. The SC was determined using Equation 1.

$$SC\ (\%) = \frac{W_1 - W_0}{W_2 - W_0} \times 100\%$$ (1)

where W_0 is aluminium foil weight (g), W_1 is aluminium foil weight containing the test sample prior to drying (g), and W_2 is aluminium foil weight containing the test sample in the wake of drying (g).

2.1.2. Gelatination time

The PU 1.2 sample is inserted into the tube. The gel time meter (Techne GT-6, Coleparmer, USA) was positioned until the needle was submerged in the sample. Furthermore, the time required for the adhesive to gelatinate was observed at 25°C. The PU 1.2 gelatination timeout is obtained when the timer stops automatically.

2.1.3. Viscosity

The 20 mL isocyanate, polyol, and PU 1.2 testing sample mixture were put into a special measuring cup (C-CC27, AntonPaar, Austria) and placed on a rotary rheometer (RheolabQC, AntonPaar, Austria). Viscosity measurements were carried out with the CC spindle no.27 with rotational speeds of 50/s, 100/s, and 150/s at 25°C to determine the average viscosity. Viscosity results are displayed with the RheoCompass app (version 1.33, AntonPaar, Austria).

2.1.4. Analysis of functional group

Fourier-Transform Infrared Spectroscopy (FTIR) (SpectrumTwo, PerkinElmer, USA) was used to analyze the functional groups of PU 1.2 in liquid and hardened form and before being reacted. Samples of isocyanate, polyol, and PU 1.2 are placed and pressed in a holder. Identification of functional groups was carried out by recording an average of 16 scans at a resolution of 4 cm^{-1} with a wavelength ranging from 400-4000 cm^{-1} at a temperature of 25 °C. The curve formation was carried out using the Universal Attenuated Total Reflectance (UATR) method. The resulting spectral patterns were displayed using the Spectrum application (version 10.5.3, PerkinElmer, USA).

2.1.5. Analysis of chemical composition

The chemical composition analysis of PU 1.2 was carried out with an integrated Gas Chromatography and Mass Spectrometry (Py-GCMS) (QP 2020 NX, Shimadzu, Japan). The

sample of 5 g PU 1.2 was pyrolyzed at 500°C for 0.10 minutes using EGA/PY-3030D multishot pyrolysis with a pressure of 20 kPa and total flow and column of 15.90 mL/minute and 0.61 mL/minute with helium as carrier gas. The temperature was 50°C for 1 minute and afterward increased to 300°C at a rate of 10°C/minute, which was maintained for up to 13 minutes. The chemical components of the pyrolysis results were detected by the NIST Library program 2017 (NIST MS Search 2.3, Adaptas Solution, USA).

2.1.6. Thermo-mechanical analysis

The PU 1.2 were spread on filter paper (CAT No. 1005-125, Whatman, England) according to the glue spread used in the application. The thermo-mechanical properties of PU 1.2 on filter paper were measured using a Dynamic Mechanical Analyzer (DMA) (DMA 8000, Perkin Elmer, USA) with dual cantilever mode with a constant recurrence pull of 1 Hz at a temperature of 25-60°C. The thermo-mechanical response is communicated concerning storage modulus (E'), loss modulus (E''), and resistance to stress (tan δ) by heating each sample at a pace of 2°C/minute. Furthermore, the isothermal investigation was done at the temperature with the highest E' for 200 minutes. The resulting graph was displayed using the Pyris Software application (version 13.3, PerkinElmer, USA).

2.2. Evaluation of Wood Characteristics

The mangium and puspa woods characteristics evaluated include physical, chemical, and surface characteristics.

2.2.1. Specific gravity

Specific gravity (SG) is measured using the Archimedes method with a $(2 \times 2 \times 2)$ cm^3 sample size. The samples were weighed under air-dry circumstances and then coated with paraffin. Samples coated with paraffin are then weighed in a water-filled container at room temperature under submerged circumstances. Furthermore, the results of the submerged weight and volume ratio are divided by the water density. The specific gravity was determined using Equation 2.

$$SG = \frac{W_1 - V_{\text{-Archimedes}}}{Density\ of\ water} \tag{2}$$

where W_1 is the weight of the sample under air-dry circumstances (g), $V_{\text{-Archimedes}}$ is the weight of the sample under submerged circumstances (cm^3), and the density of water is 1 g/cm^3.

2.2.2. Density, moisture content, and volume shrinkage

Measurement of density and moisture content (MC) refers to ASTM D-143 (American Society for Testing Materials 2014). Samples measuring $(2 \times 2 \times 2)$ cm^3 were measured in volume, weighed under air-dry circumstances, and dried at a temperature of 103 ± 2°C to a constant weight. The sample volume in the dry condition was measured and weighed again. Density under dry and kiln-dry circumstances, MC, and shrinkage were determined using Equations 3–6.

$$Air\text{-}dry\ density\ (g/cm^3) = \frac{W_1}{V_1} \tag{3}$$

$$Kiln\text{-}dry\ density\ (g/cm^3) = \frac{W_2}{V_2} \tag{4}$$

$$MC\ (\%) = \frac{W_1 - W_2}{W_2} \times 100\% \tag{5}$$

$$Shrinkage\ (\%) = \frac{V_1 - V_2}{V_2} \times 100\% \tag{6}$$

where W_1 is the weight of the sample under air-dry condition (g), V_1 is the volume of the sample under air-dry condition (cm^3), W_2 is the weight of the sample under kiln-dry condition (g), and V_2 is the volume of the sample under kiln-dry condition (cm^3).

2.2.3. Extractive content and pH

Extractive measurements were carried out using three solvents, namely 25°C water, boiling water, and 1% NaOH. Measurement of 25°C water-soluble extractive content refers to TAPPI T207 CM-08 (TAPPI 2007). The sample of 2 g 40-60 mesh sawdust was immersed in 300 mL of refined water for 48 h. The sample was then sifted with refined water and dried at a temperature of 103 ± 2°C to constant weight.

The measurement of the dissolved extractive content of boiling water refers to TAPPI T207 CM-08 (TAPPI 2007). The 2 g 40-60 mesh sawdust sample was immersed in 100 mL of boiling refined water for 3 h. Powder immersion filtrate in refined water was tested using a pH meter (PH-016, Hbbossen, China) to measure the pH. The sample was then sifted with boiling distilled water and afterward dried at a temperature of 103 ± 2°C until it reached a constant weight.

The measurement of 1% NaOH soluble extractive content refers to TAPPI T212 OM-18 (TAPPI 1993). The sample of 2 g 40-60 mesh sawdust was immersed in 100 mL 1% NaOH and boiled for 1 h. The samples were stirred for 10, 15, and 25 minutes after soaking. The sample was then sifted with boiling distilled water and 10% acetic acid twice and dried at 103 ± 2°C to constant weight. The extractive content of each invention was determined using Equation 7.

$$Extractive\ content\ (\%) = \frac{W_1 - W_2}{W_2} \times 100\% \tag{7}$$

where $W1$ is the weight of the sawdust sample before extraction (g), and W_2 is the weight of the sawdust sample in the wake of extraction (g).

2.2.4. Surface roughness

Surface roughness measurement refers to ISO 4287 (International Organization for Standardization 1997) using a surface roughness tester (SJ210, Mitutoyo, Japan). The cutoff length for the sample is 0.80 mm with a track length of 6 mm and a measurement speed of 0.50 mm/second. Measurements were done pursuing the direction perpendicular to the grain and were carried out at five different points on the sample surface. Surface roughness measurement parameters are expressed as arithmetical mean roughness (Ra).

2.2.5. Wettability

Wettability estimation involving boundaries as the contact point between the adhesive and wood using the sessile drop technique for three repetitions. The adhesive is dripped using an injection with a liquid volume of 0.02 mL on the wood sample. The droplet results were recorded for 180 seconds and observed under a microscope (XSP-13AE, Yazumi, China). The recorded video is cut using the GOM player application (version 2.3 Plus, GOM and Company, Germany)

in augmentations of 10 seconds. The contact point of each picture piece was estimated using the ImageJ application (version 1.53k, National Institutes of Health, USA) with drop snake plugins analysis. Constant contact angle values were set between time and contact angle using SAS (Version 9.0, SAS Institute, USA). The value of the wettability rate (K) was resolved given the Shi and Gardener (S/G) model (Shi and Gardner 2001) using the XLSTAT program (Version 14, Addinsoft Inc., USA). The S/G model proposes Equation 8.

$$\theta \ (°) = \frac{\theta i . \theta e}{\theta i + (\theta e - \theta i) \ exp[K(\theta e \ / \theta e - \theta i) \ t]} \times 100\%$$ (8)

where θi is the underlying contact angle (°), θe is the equilibrium contact angle (°), K is dynamic wettability, and t is time (second).

2.3. Manufacturing and Testing of CLT

The wood is formed into laminates that have been sorted refers to JAS 3079 (Japanese Agricultural Standard 2019) and applied with adhesive of 160 g/m², then arranged perpendicular to the grain between layers and compressed with a 0.80 MPa pressure for 200 minutes (Liao et al. 2017) to form CLT with (100 × 30 × 3.60) cm³ size. An illustration of lamina size and CLT orientation is shown in **Fig 1**.
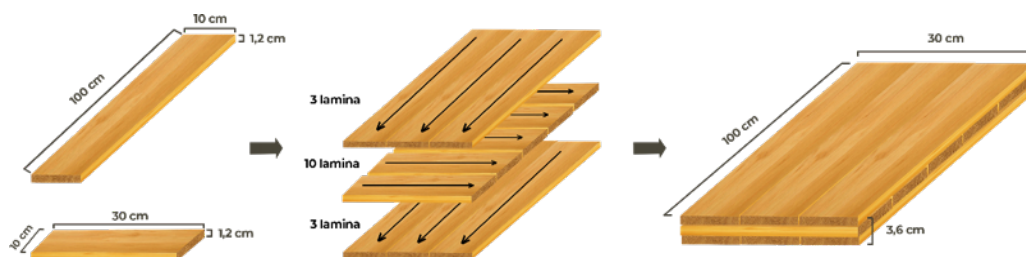
Fig. 1. Size and layer orientation of CLT.

The CLT test refers to the JAS 3079 standard (Japanese Agricultural Standard 2019) with parameters of density, moisture content, shrinkage, water absorption (WA), thickness swelling (TS), water delamination (WD), boiling delamination (BD), modulus of elasticity (MOE), modulus of rupture (MOR), block shear test parallel to the grain, and block shear test perpendicular to the grain. In addition, the type of failure that occurred in the mechanical test was also observed. Based on these tests, the CLT cutting pattern and the study's sample dimensions are shown in **Fig. 2**, consisting of: (A) sample of density, MC, and shrinkage test (7.50 × 7.50 × 3.60) cm³, (B) sample of WA, TS, and WD test (7.50 × 7.50 × 3.60) cm³, (C) sample of BD test (7.50 × 7.50 × 3.60) cm³, (D) backup sample test (7.50 × 7.50 × 3.60) cm³, (E) sample of MOE and MOR test (85 × 30 × 3.60) cm³, (F) sample of block shear test perpendicular to the grain (8 × 4 × 3.60) cm³, and (G) sample of block shear test parallel to grain (8 × 2.50 × 3.60) cm³.

Fig.2. Cutting example of CLT in this research.

2.3.1. Test of density, MC, and shrinkage

The dimensions of test sample A were measured under air-dry circumstances to obtain the volume value (V_1). Samples with air-dry circumstances were then weighed to obtain air-dry weight (W_1). The density value was determined using Equation 9.

$$Density \ (kg/m^3) \ = \ \frac{W_1}{V_1} \tag{9}$$

Test sample A was dried at a temperature of $103 \pm 2°C$ until the weight was constant (W_1). The samples with kiln-dry circumstances were weighed to obtain the kiln-dry weight (W_2). The value of moisture content (MC) was determined using Equation 10.

$$MC \ (\%) \ = \ \frac{W_1 - W_2}{W_2} \times 100\% \tag{10}$$

The initial (V_1) and oven-dried volume (V_2) of the sample after kiln-drying were measured. The percentage of volume shrinkage was determined using Equation 11.

$$Volume \ Shrinkage \ (\%) \ = \ \frac{V_1 - V_2}{V_2} \times 100\% \tag{11}$$

where W_1 is the weight of the sample under air-dry condition (g), V_1 is the volume of the sample under air-dry condition (cm^3), W_2 is the weight of the sample under kiln-dry condition (g), and V_2 is the volume of the sample under kiln-dry circumstances (cm^3).

2.3.2. Test of dimensional stability

Test sample B was weighed initially and measured for thickness on all sides in air-dry conditions and then immersed in water at room temperature for 24 h. The soaked samples were then weighed in wet conditions. The percentage of WA was determined using Equation 12.

$$WA \ (\%) \ = \ \frac{W_2 - W_1}{W_1} \times 100\% \tag{12}$$

The soaked sample was then measured for thickness in wet condition. The percentage of thickness development was determined using Equation 13.

$$TS \ (\%) \ = \ \frac{T_2 - T_1}{T_1} \times 100\% \tag{13}$$

where W_1 is the weight of the sample under air-dry condition (g), T_1 is the thickness of the sample under air-dry condition (cm), W_2 is the weight of the sample after immersed (g), and T_2 is the thickness of the sample after immersed (cm).

2.3.3. Test of delamination against cold and boiling water

Test sample B measured the length of the straight and cross bond lines on each side and added up (Σ adhesive line). Next, the samples were immersed in water at room temperature for 24 h, then dried at $70 \pm 3°C$ until the weight was constant. After that, the length of the peeling adhesive line was measured on all sides and added (Σ the peeling adhesive line). The delamination value was determined using Equation 14.

$$Delamination \ (\%) \ = \ \frac{\Sigma \ the \ peeling \ adhesive \ line}{\Sigma \ adhesive \ line} \times 100\% \tag{14}$$

Test sample C was immersed in boiling water for 4 h with a water bath (WNB 10, Memmert, Germany), then immersed in water at room temperature for 1 h. Next, the sample was dried at a

temperature of 70 ± 3°C to a constant weight. The sample delamination percentage is calculated using a formula such as the water delamination test.

2.3.4. Test of MOE and MOR

Test sample E was loaded using UTM Baldwin (Baldwin, USA) by two-point loading with a span of 76 cm. The loading speed given is 14.7 MPa/minute until the sample breaks. The type of failure that occurs in the sample is observed. MOE and MOR values were determined using Equations 15 and 16.

$$MOE \ (MPa) = \frac{23\Delta Pl^3}{108bh^3\Delta y} \times 10^{-3} \tag{15}$$

$$MOR \ (MPa) = \frac{Pl}{bh^2} \tag{16}$$

where l is the span (mm), b is the width of sample (mm), h is the thickness of the sample (mm), P is the maximum load (N), ΔP is the difference between the upper and lower load in proportion limit (N), and y is the difference of deflection from the top and bottom load (mm).

2.3.5. Test of shear strength

Test sample F was cut to leave the surface part wide, and the G test sample was cut in the thick direction. Next, one side at the end is formed, as shown in **Fig. 3**.
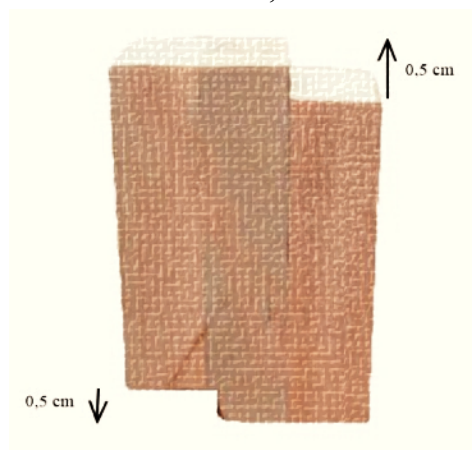
Fig.3. Sample of block shear test.

The sample was then pressurized with UTM Shimadzu (AG-IS 50 kN, Shimadzu, Japan) in both directions at 7.90 MPa/minute for the F test sample and 15.70 MPa/minute for the G test sample. The type of failure that occurred in the sample was observed. The value of the shear strength of the block sample was determined using Equation 17.

$$Shear \ strength \ (MPa) = \frac{P}{A} \tag{17}$$

where P is load when the sample breaks (N), and A is strain area (mm^2).

2.4. Data Analysis

Data analysis in this study used a completely randomized design with a single treatment at two testing stages in the effect of the wood characteristics on the penetration of PU 1.2 and the effect of the layer combination on the quality of the resulting CLT. Factors applied to the wood

characteristic test of CLT material are variations in wood species, namely mangium and puspa, with five repetitions of the level. The factors applied to the CLT quality test are variations in the layer combination (face-core-back) in the form of mangium-mangium-mangium (MMM), puspa-puspa-puspa (PPP), mangium-puspa-mangium (MPM), and puspa-mangium-puspa (PMP) with three repetitions. The analysis was also applied to several adhesive tests to determine the success of the PU 1.2 formulation. Factor effect on observations was seen using the Analysis of Variance (ANOVA) at a 95% confidence level. Duncan's Multiple Range Test (DMRT) was carried out to determine the difference between the levels of the factor that affected the response. Analyzes were performed with the IBM SPSS Statistics computer program (Version 26, SPSS Inc., USA). The data from the analysis were then compared with the JAS 3079 standard.

3. Results and Discussion

3.1. Characteristics of Adhesive

The PU 1.2 was successfully formulated from the reaction of isocyanates and polyols with quite different characteristics from the commercial products. The appearance of PU 1.2 from the reaction of isocyanate and polyol is visually shown in **Fig.4**.
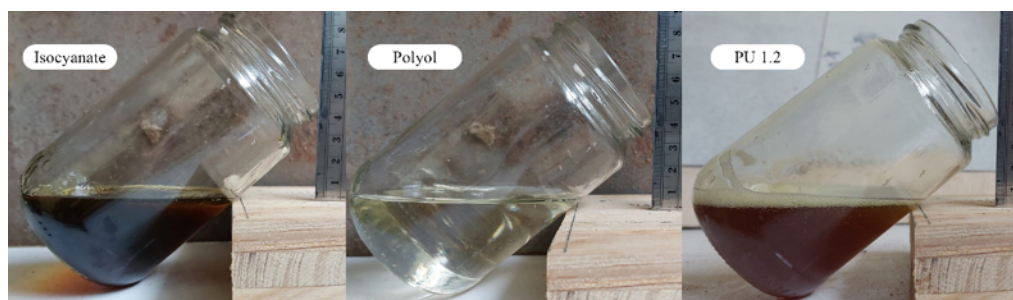
Fig.4. Visual appearance of isocyanates, polyols, and PU 1.2.

Several parameters, including SC, viscosity, FTIR, Py-GCMS, and thermo-mechanical analysis, indicate the success of the PU 1.2 formulation. The SC, along with the gelatinization time of PU 12 and its constituent materials, are shown in **Table 1**. Isocyanate is the highest SC value, followed by PU 1.2 and polyol. DMRT results show a significant difference in SC between the polyol and PU 1.2. Other studies have also reported significant differences in polyurethane SC with its constituent materials (García-Pacios et al. 2011; Liu et al. 2019).

Table 1. The SC of isocyanate, polyol, and PU 1.2 and their gelatinization time

Characteristics	Value
SC (%)	
- Isocyanate	99.47 ± 0.53^b
- Polyol	86.73 ± 6.61^a
- PU 1.2	95.40 ± 0.14^b
Gelatinization time (minute) at 25°C	182.10

Notes: Numbers in the same column followed by different letters mean that they have significantly different values from the ANOVA results ($\alpha = 0.05$). Data is the mean value of n = 3.

The difference is due to the formation of urethane resulting from the reaction of isocyanates and polyols (Szycher 2012). The research of Hass et al. (2012) also reported the potential for

synthetic polyurethane adhesives with SC approaching 100%. Higher levels of adhesive solids can increase adhesion, affecting composite wood's mechanical quality (Moslemi et al. 2020). In addition, the gelatinization time of PU 1.2 from the reaction of isocyanate and polyol was 182.10 minutes at room temperature. This range is still in the time of efficient CLT compression using polyurethane adhesive, which is 200 minutes (Liao et al. 2017). Based on SC and gelatinization time parameters, PU 1.2 adhesive is compatible to be applied in this study. Another parameter that can determine the compatibility of PU 1.2 to CLT manufacturing is the viscosity shown in **Fig. 5**.

(a)   (b)

(c)
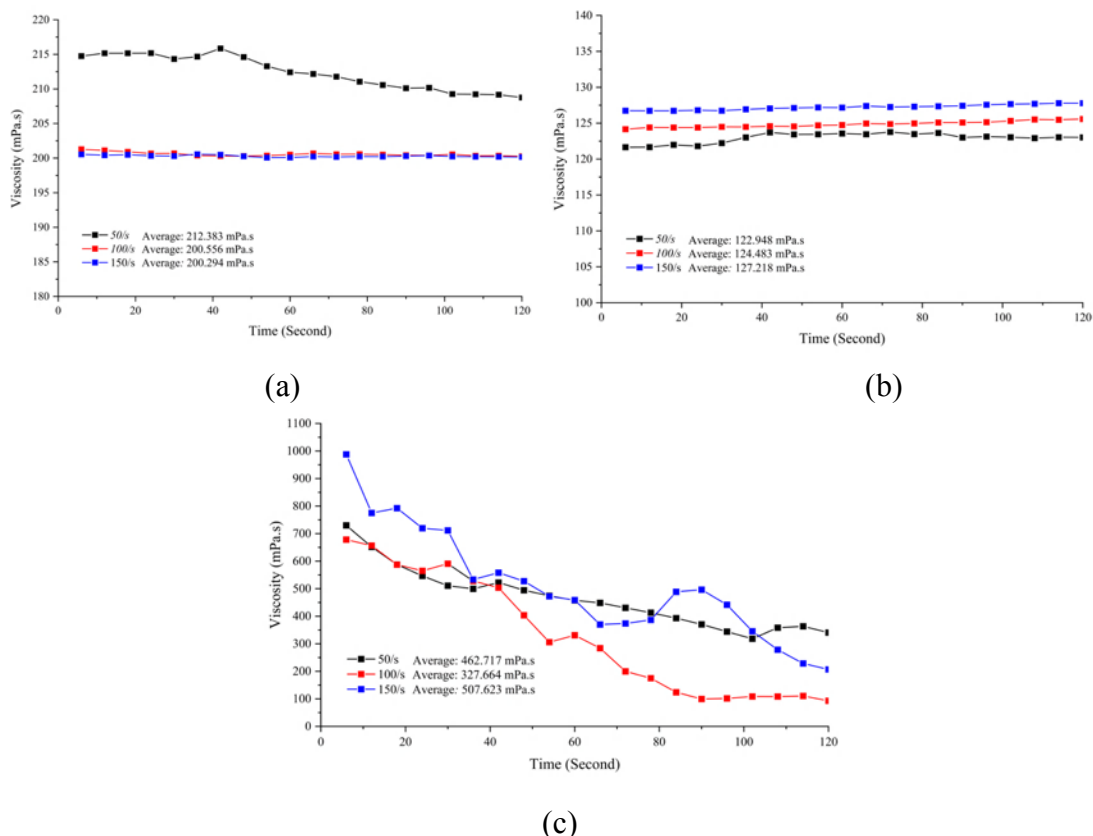
Fig. 5. Viscosity of (a) isocyanates, (b) polyols, (c) and PU 1.2 in variations of rotational speed.

The graphs in **Fig. 5** show the variation in the average viscosity between isocyanates and polyols with PU 1.2. The reaction between isocyanates with an average viscosity of 200.29-212.38 mPa.s and polyols with an average viscosity of 122.95-127.22 mPa.s produced PU 1.2 with an average viscosity of 327.66-507.62 mPa.s. The average viscosity of PU 1.2 is also higher than that of commercial PU (1.0) by 150-250 mPa.s. The average viscosity of PU 1.2, which is higher than commercial, is due to the increase in the molecular weight of the isocyanate (Aristri et al. 2022; Lubis et al. 2022; Szycher 2012). The graphs in **Fig. 5** also show different trends between PU 1.2 and its constituent materials. The isocyanate and polyol graphs tend to be constant with increasing viscosity along with the rotational speed, while the PU 1.2 graphs tend to decrease with time. The low viscosity at the beginning of the reaction will facilitate the penetration of the adhesive on the substrate (Radabutra et al. 2020) so that PU 1.2 can be sown well on CLT laminae at room temperature. This is due to a change in the characteristics of the functional groups shown in **Fig. 6**.
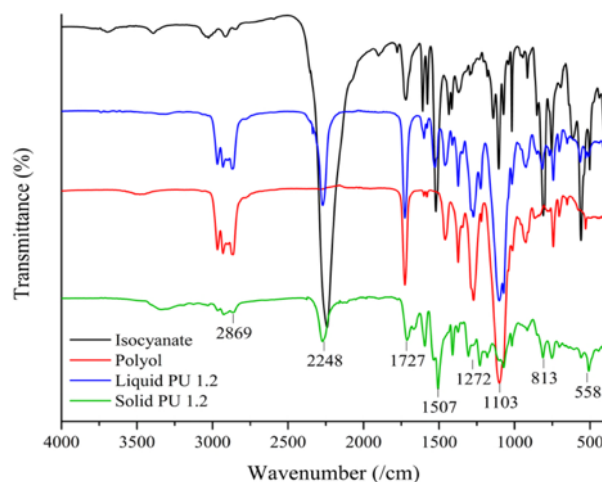
Fig. 6. Characteristics of PU 1.2 in solid and liquid conditions and their constituent materials based on the results of FTIR.

The graph in **Fig. 6** shows several peaks of liquid PU 1.2 and solid PU 1.2, indicating isocyanate and polyol content. This can be seen from the peak of N=C=O at 2248 cm^{-1} and the formation of urethane bound at numbers 1460-1600 cm^{-1} and urethane linkages at numbers 1600-1720 cm^{-1}. Details of the differences in the functional groups of isocyanate, polyol, liquid PU 1.2, and solid PU 1.2 are summarized in **Table 2**.

Table 2. Summary of FTIR analysis results of isocyanates, polyols, liquid PU 1.2, and solid PU 1.2

Wavenumber (cm^{-1})				Functional Groups	References
Isocyanate	**Polyol**	**Liquid PU**	**Solid PU**		
2869	2869	2869	2869	C–H	2800-3000 cm^{-1} (Gurunathan et al. 2015)
2248	-	2248	2248	N=C=O	2230-2276 cm^{-1} (Poh et al. 2014; Oliviero et al. 2019)
1727	1727	1727	1727	C=O	1664-1780 cm^{-1} (Gurunathan et al. 2015)
1507	1507	1507	1507	Urethane bond	1460-1600 cm^{-1} (Thébault et al. 2015)
1272	1272	1272	1272	C–N (Amida II band)	1200-1500 cm^{-1} (Sunija et al. 2014)
1103	1103	1103	1103	Secondary O–H	1100-1200 cm^{-1} (Hazmi et al. 2013; Kong et al. 2011)
813	813	813	813	C–H	810-950 cm^{-1} (Chen et al. 2019)
558	558	558	558	N–H	400-800 cm^{-1} (Delpech and Miranda 2012)

The graph of liquid PU 1.2 has the highest peak at 1103 cm^{-1}, indicating the presence of secondary O–H groups and urethane linkages at the peak number of 1727 cm^{-1}. The steepness of the urethane linkages and secondary O–H caused a decrease in the viscosity of the PU 1.2 reaction within 120 seconds in **Fig. 6**. On the other hand, the solid PU 1.2 FTIR graph shows a significant decrease in the peaks of the N=C=O and secondary O–H groups but retains the peaks of the urethane bound to the wavenumber of 1507 cm^{-1}. This is due to the condition of PU 1.2, which has thickened and leaves a bound group so that its reactivity decreases. In addition to functional group

analysis through FTIR, the chemical components of PU 1.2 can be identified in more detail through the Py-GCMS results shown in **Fig. 7** and **Table 3**.
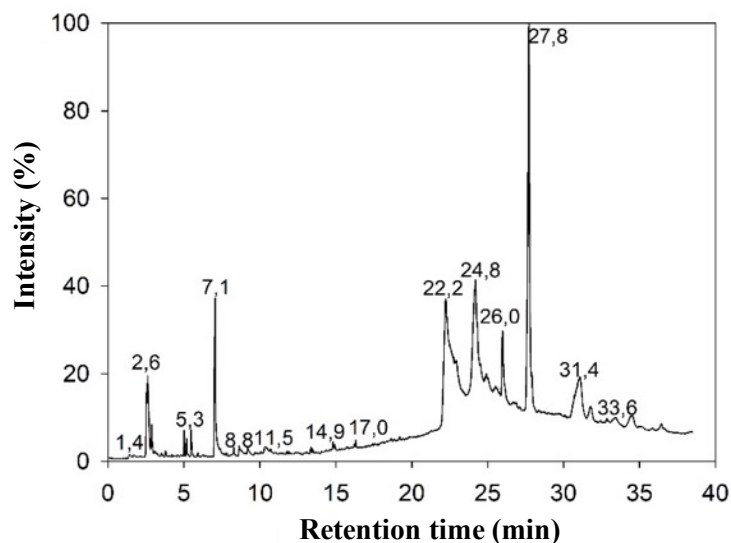
Fig. 7. Intensity graph of PU 1.2 composition within a certain retention time.

Table 3. Details of the PU 1.2 compound from Py-GCMS

Peak Number	Retention (minute)	Molecular Weight (m/z)	Compound*
1	2.53	44	Carbdioxideida
2	2.61	41	Acetonitrile
3	2.86	43	Ethylenimine
4	3.80	43	Ethylenimine
5	5.10	70	1-Pentene
6	5.17	45	Dimethylamine
7	5.48	43	Ethylenimine
8	7.05	57	Methane, isocyanato-
9	8.28	59	Propilamine
10	13.36	41	Acetonitrile
11	14.82	41	Acetonitrile
12	14.93	57	Methane, isocyanato-
13	16.30	57	Methane, isocyanato-
14	22.26	43	Ethylenimine
15	22.61	239	Benzenaminy, N,N-dimethyl-4-[(3-methylfenyl)azo]-
16	22.76	239	Benzenaminy, N,N-dimethyl-4-[(3-methylfenyl)azo]-
17	24.19	55	Propanenitrile
18	24.56	59	Propilamine
19	24.84	43	Ethylenimine
20	24.93	96	3-Furaldehyde
21	25.04	96	3-Furaldehyde
22	25.99	43	Ethylenimine
23	27.72	149	Benzenaetanamine, N,α-dimethyl-
24	27.89	96	3-Furaldehyde
25	30.71	43	Ethylenimine
26	30.97	43	Ethylenimine
27	31.06	43	Ethylenimine
28	31.76	57	Methane, isocyanato-
29	34.51	240	9,10-Anthracenedione, 1,4-dihydroxy-
30	36.45	96	3-Furaldehyde

Notes: identification of the compound was based on previous studies (Dyer and Read 1961; Dyer and Wright 1959; Zhang et al. 2009).

The graph in **Fig. 7** shows some of the dominant peaks of the 38-minute retention time. The highest peak was seen at 27.8 minutes containing benzeneethanamine, N,α-dimethyl- and 3-furaldehyde compounds, then at 24.6 minutes indicating propylamine, at 22.25 minutes indicating ethyleneimine, at 7.10 minutes indicating indicates methane, isocyanate. In addition to these peaks, several retention times with fairly high intensity are described in **Table 3**.

The data in **Table 3** shows the results of Py-GCMS in polyurethane formation and degradation. The reaction for the formation of a polyurethane according to Dyer and Wright (1959) and Dyer and Read (1961), is as follows:

$$R\!-\!N\!=\!C\!=\!O \ + \ H\!-\!O\!-\!R' \longrightarrow R\!-\!\underset{\underset{H}{|}}{N}\!-\!\overset{\overset{O}{\|}}{C}\!-\!O\!-\!R' \tag{1}$$
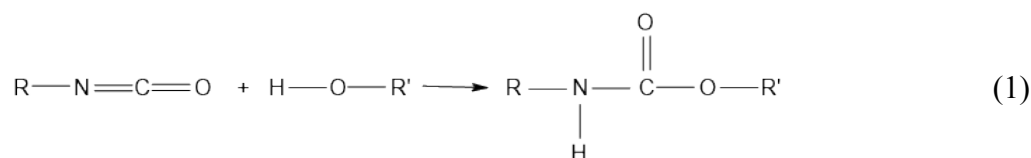
The formation reaction was characterized by the presence of peak number 8 (–N=C=O) and peak number 29 (–OH), which formed polyurethane with urethane along with several forms of degradation, including:

$$R\!-\!\underset{\underset{H}{|}}{N}\!-\!\overset{\overset{O}{\|}}{C}\!-\!O\!-\!R' \longrightarrow R\!-\!N\!=\!C\!=\!O \ + \ H\!-\!O\!-\!R' \tag{2}$$

$$R\!-\!\underset{\underset{H}{|}}{N}\!-\!\overset{\overset{O}{\|}}{C}\!-\!O\!-\!CH_2\!-\!CH_2\!-\!R' \longrightarrow R\!-\!NH_2 \ + \ CO_2 \ + \ CH_2\!=\!CH\!-\!R \tag{3}$$

$$R\!-\!\underset{\underset{H}{|}}{N}\!-\!\overset{\overset{O}{\|}}{C}\!-\!O\!-\!R' \longrightarrow R\!-\!\underset{\underset{H}{|}}{N}\!-\!R' \ + \ CO_2 \tag{4}$$
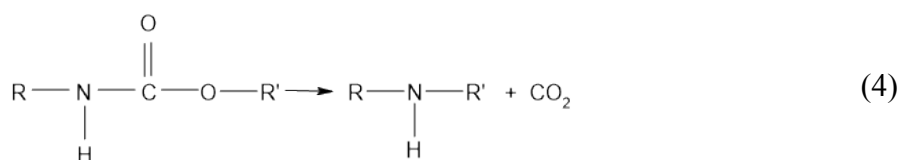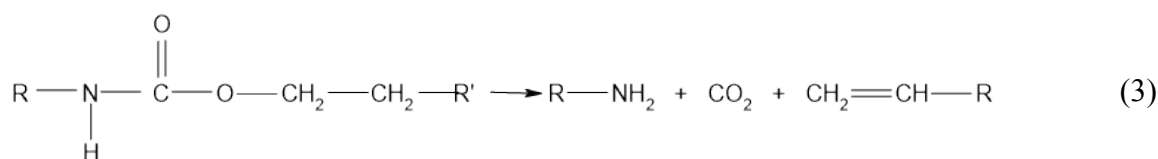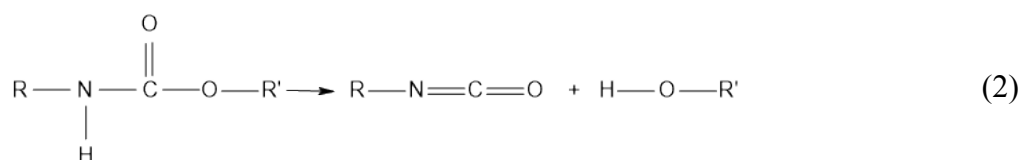
Peak numbers 8, 12, 13, and 18 (–N=C=O); peak numbers 5, 20, 21, 24, and 30 (chain O); and peak number 29 (–OH) indicates the second polyurethane degradation product, which is the reverse of the formation process. In addition, peaks number 3, 4, 7, 14, 19, 22, 25, 26, and 27 (–NH$_2$); peak number 2, 10, 11, 15, 16, and 17 (N chain); peak number 23 (–NH–); and peak number 1 (O=C=O) indicates the fourth polyurethane degradation product. However, the absence of the CH$_2$=CH bond indicated that the third polyurethane degradation did not occur. The high-intensity peak number 23 (–NH–) indicates the presence of urethane groups before and after degradation due to high temperatures. The response of PU 1.2 to lower temperatures is shown in the thermo-mechanical graph in **Fig. 8**.

The graph in **Fig. 8** (a) shows the highest E' PU 1.2 value of 114.21 GPa at a temperature of 35.48°C. This indicates the temperature of PU 1.2 with the best thermo-mechanical capability. The graph trend in **Fig. 8** (a) shows a decrease in the value of E' after the peak and a tendency to increase in the value of E". High E" value is positively correlated with adhesive stiffness or viscosity (Naresh et al. 2018; Ravi-Sankar et al. 2011). In addition, the increasing trend of the tan δ graph, which represents the damping ability (Menard 2008), is also seen in **Fig. 8** (a). These thermo-mechanical characteristics indicate the potential for compaction of PU 1.2 molecules

above a temperature of 35.48°C. Other studies have experienced premature adhesive hardening due to temperature factors to minimize the time of liquid penetration and the formation of mechanical bonds to wood (Bekhta et al. 2020). Adjusting for the optimal compression time of CLT using polyurethane (Liao et al. 2017), the trend of E' PU 1.2 at 35°C for 200 minutes in **Fig. 8** (b) does not show significant fluctuations after ± 60 minutes. However, the graph, which still tends to increase at 200 minutes, shows a better potential for E' at > 200 minutes. Overall, PU 1.2 adhesive can penetrate and harden at a temperature of 35°C for 200 minutes.
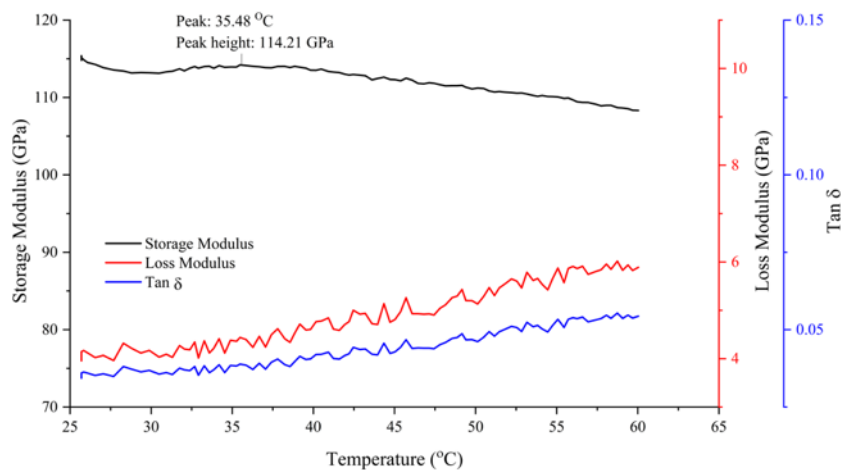
(a)
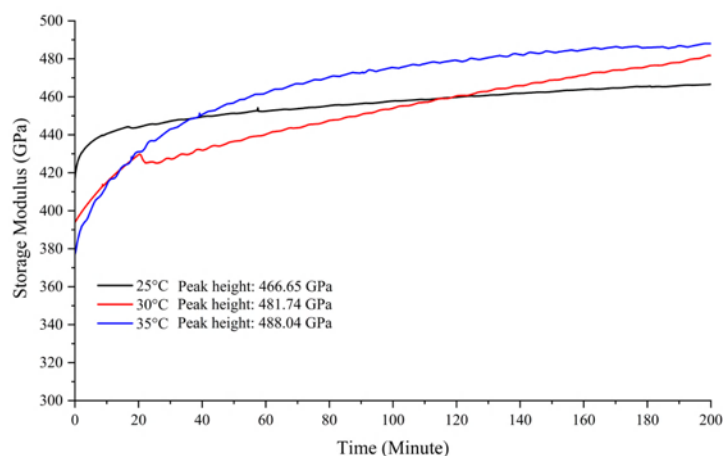
(b)

Fig. 8. Thermo-mechanical response of PU 1.2 in variations of (a) temperature and (b) time.

3.2. Characteristics of CLT Wood Materials

The wood characterization of CLT material was carried out through several parameters, including physical properties, chemical content, and surface characteristics. Mangium and puspa wood as CLT materials in this study had several characteristics that were significantly different. The physical characteristics of mangium and puspa wood are shown in **Table 4**.

The data in **Table 4** shows SG and density in air-dry and kiln-dry conditions of puspa wood which are higher than mangium. The ANOVA results showed differences in wood species, which significantly affected the value of SG, density, MC, and shrinkage. Mangium wood has an SG of 0.45-0.49. In several other studies, this value is still in the SG range of mangium (Karlinasari et

al. 2021; Lokmal 2010). On the other hand, puspa wood has an SG of 0.53-0.57. This value tends to be below SG of puspa in several other studies, that is, 0.57-0.61 (Hadjib et al. 2010). However, SG of mangium and puspa still meet the standard for CLT raw materials of 0.35 (American National Standards Institute 2018).

Table 4. Physical characteristics of CLT wood material

Characteristics	Mangium		Puspa	
	Heartwood	Sapwood	Heartwood	Sapwood
SG	0.49 ± 0.01^{ab}	0.45 ± 0.08^{a}	0.57 ± 0.02^{c}	0.53 ± 0.01^{bc}
Density (g/cm³)				
Air-Dry	0.56 ± 0.03^{b}	0.46 ± 0.03^{a}	0.72 ± 0.03^{c}	0.69 ± 0.03^{c}
Kiln-Dry	0.55 ± 0.03^{b}	0.44 ± 0.03^{a}	0.72 ± 0.02^{c}	0.69 ± 0.03^{c}
MC (%)	14.24 ± 0.17^{a}	13.79 ± 1.22^{a}	15.82 ± 3.61^{b}	15.63 ± 0.47^{b}
Shrinkage (%)				
Radial	3.71 ± 0.89^{ab}	2.69 ± 0.64^{a}	4.95 ± 1.91^{b}	4.71 ± 0.53^{b}
Tangential	6.28 ± 0.74^{ab}	4.76 ± 0.66^{a}	9.29 ± 1.11^{c}	6.89 ± 1.97^{b}

Notes: numbers in the same column followed by different letters mean that they have significantly different values from the ANOVA results ($\alpha = 0.05$). Data is the average value of n = 5.

The significantly different values of mangium and puspa MC in **Table 4** did not significantly impact CLT. This is because all samples are in the standard range of the American National Standards Institute (2018), which is 15%. Other physical properties of puspa also tend not to differ significantly between parts, so the application of heartwood and sapwood on CLT can be applied. On the other hand, DMRT proved a significant difference between the air-dry and kiln-dry density of mangium on the heartwood and sapwood. The mangium heartwood with a wall thickness and fiber diameter higher than that of sapwood is the main factor in differentiating the density between sections Nugroho et al. (2012). Therefore, mangium heartwood is more suitable to be used as a CLT material than sapwood.

Another physical characteristic that becomes an important parameter of CLT material is shrinkage. Based on DMRT in **Table 4**, the shrinkage of the puspa was significantly different from that of acacia in both parts. This is because the SG of puspa is high, so the cell wall space to be filled with water is wider (Priadi et al. 2019; Rowell and Youngs 1981). The value of shrinkage and SG of puspa, which was higher than mangium, indicated the importance of the combination with mangium in the preparation of CLT to equalize the quality. Apart from these things, shrinkage is also potentially influenced by wood extractive content and pH, as shown in **Table 5**.

Table 5. Extractive content and pH of CLT wood material

Characteristics	Mangium	Puspa
Extractive (%)		
Room Temperature Water	7.19 ± 0.32^{a}	6.06 ± 0.43^{b}
Boiling Water	9.58 ± 0.49^{a}	7.25 ± 0.51^{b}
1% NaOH	22.70 ± 2.23^{a}	14.68 ± 0.78^{b}
pH	5.05 ± 0.42^{a}	6.11 ± 0.05^{b}

Notes: numbers in the same column followed by different letters mean that they have significantly different values from the ANOVA results ($\alpha = 0.05$). Data is the average value of n = 5.

The data in **Table 5** shows the extractive content of mangium, which is higher than puspa in the three solvents. The ANOVA results showed that different types of wood significantly affected

extractive content and pH. High extractives significantly correlate with decreased wood shrinkage (Bossu et al. 2016; Jankowska et al. 2017; Priadi et al. 2019), so the dimensions of mangium are more stable than puspa. Generally, acidic pH indicates high extractives that affect dimensional stability. However, extractives also have the potential to prevent the penetration of PU 1.2 in wood. The penetration behavior of PU 1.2 against mangium and puspa wood is shown in **Fig. 9**.
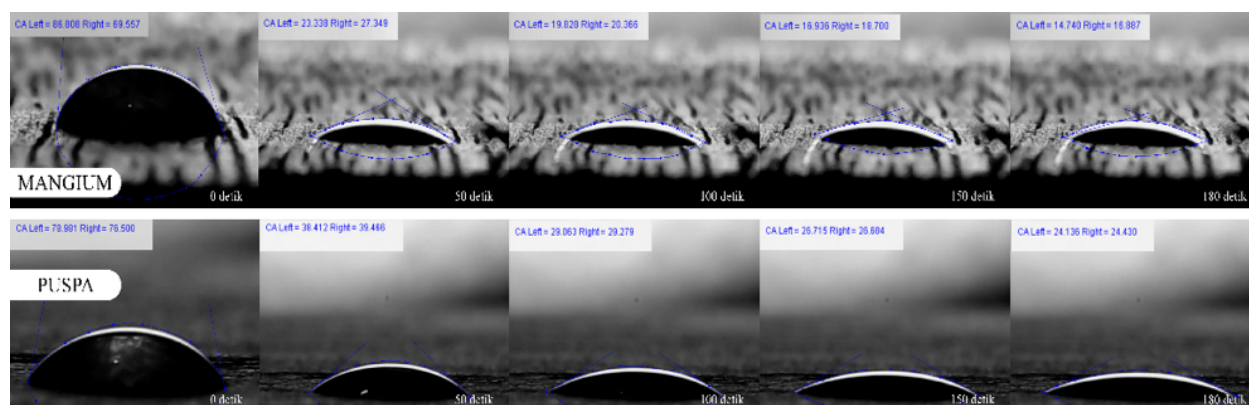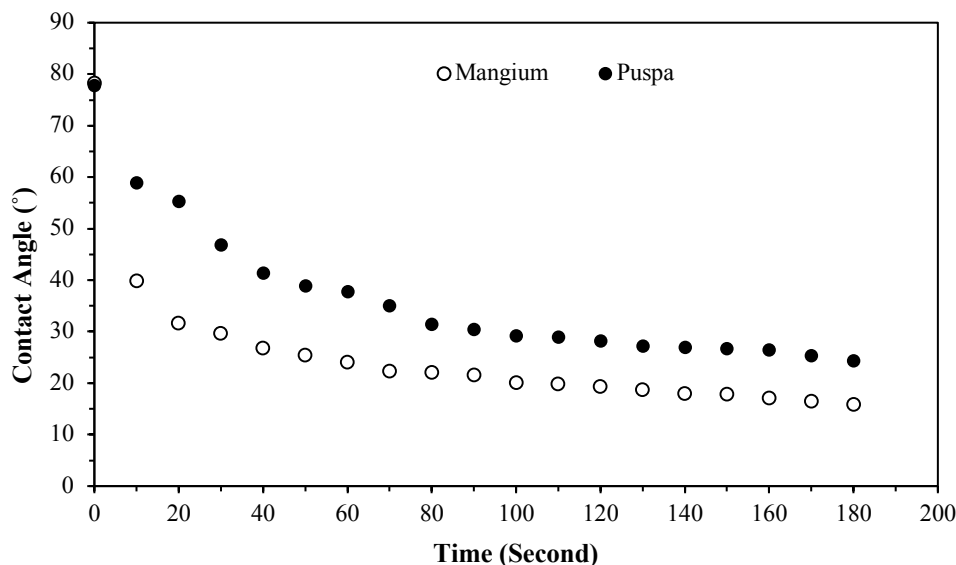
Fig. 9. Graphics and portraits of PU 1.2 contact angles on mangium and puspa wood.

The graph in **Fig. 9** shows a downward trend in the contact angle of PU 1.2 for mangium wood, which is lower than for puspa wood. The θi of mangium and puspa wood tends to be the same in the range of 77-78°. However, the contact angle of PU 1.2 with mangium wood starts to reach θe at 19.33° while that of puspa wood at 26.72° which can be seen visually in the portrait in **Fig. 9**. The data shows that the penetration ability of PU 1.2 on mangium wood is better than puspa. This result is inversely related to the effect of wood extractives and pH on liquid penetration (Bossu et al. 2016). This may be due to the complex correlation between extractive and adhesive wettability (Nussbaum and Sterley 2002). In addition, the particle size of polyurethane also tends to be stable in the pH range of 5-12 (Lai et al. 2021), so the pH of the wood material in this study does not affect PU 1.2. Therefore, the difference in contact angle between mangium and puspa is more easily explained through the surface roughness parameters between the two wood species, as shown in **Table 6**.

Table 6. Surface characteristics of CLT wood materials

Characteristics	Mangium	Puspa
Ra (µm)	8.74 ± 1.30^a	7.87 ± 0.78^a
θe (°)	19.33 ± 2.57^a	26.72 ± 0.65^b
K	0.12 ± 0.01^a	0.09 ± 0.05^a

Notes: numbers in the same column followed by different letters mean that they have significantly different values from the ANOVA results ($\alpha = 0.05$). Data is the average value of n = 3.

Table 6 shows that the Ra of mangium is higher than puspa wood. The value of Ra is positively correlated with the value of K PU 1.2 for both types of wood. Although the ANOVA results did not show a significant effect of the two types of wood, several other studies proved a positive correlation between surface roughness and wettability rate (Darmawan et al. 2018; Karlinasari et al. 2018). The insignificant difference in K between the two types of wood can potentially reduce the adhesive interaction effect on mangium or puspa wood on CLT quality. Based on this, the CLT quality in each sample is determined more by the basic quality of the wood material than by the interaction of the adhesive on the wood.

3.3. Characteristics of CLT

3.3.1. Physical properties of CLT

The CLT characterization was performed using MMM, PPP, MPM, and PMP layers. The results showed the effect of different layer combinations on several physical parameters of CLT. One of the basic physical parameters that experience this is the density shown in **Fig. 10**.
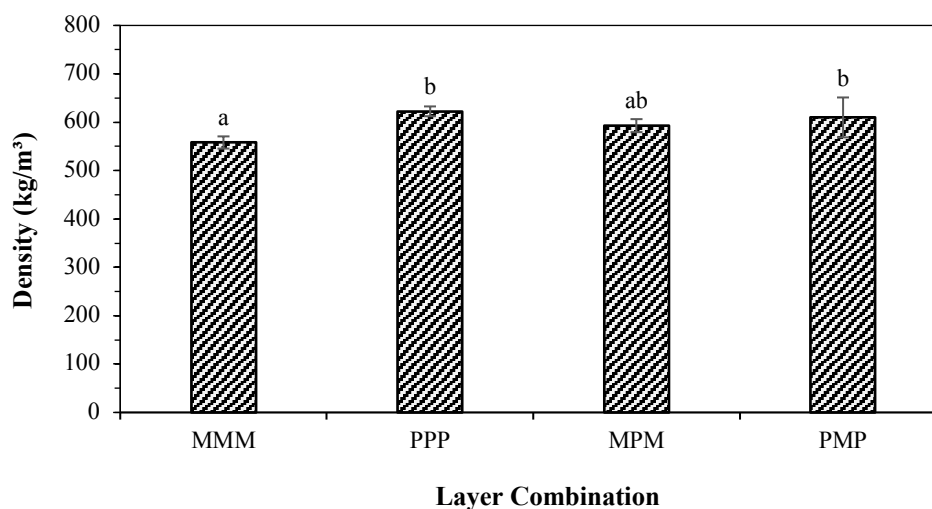
Fig. 10. Density of CLT in the variation of layer combination (Graphs with the same color or bar pattern but followed by different letters mean that they have significantly different values from the ANOVA results ($\alpha = 0.05$). Data is the mean value of n = 3).

The graph in **Fig. 10** shows the highest density in the PPP CLT sample of 662.50 kg/m^3 followed by the PMP CLT of 609.90 kg/m^3, the MPM CLT of 592.89 kg/m^3, and CLT MMM with the smallest value of 558.07 kg/m^3. The ANOVA results showed a significant effect of different layer combinations on the CLT density value. DMRT proved a significant difference between MMM CLT with PPP CLT and PMP CLT. The significant difference between the CLT density is in line with the significant variation in material density in air-dry and kiln-dry conditions (**Table**

4). The results in **Fig. 10** also prove that the density increases with the combination of puspa wood. Several other studies also showed a significant increase in CLT density in wood species with higher densities (Corpataux et al. 2020; Yusoh et al. 2021). In addition, the density value of MMM CLT tends to increase compared to the air-dry and kiln-dry density of mangium wood. This has the potential to occur in low-medium-density wood due to the densification process during CLT compression, which impacts improving mechanical quality (Feng and Chiang 2020). Despite having different densities, each CLT has a more stable MC and volume shrinkage in **Fig. 11**.

(a)

(b)
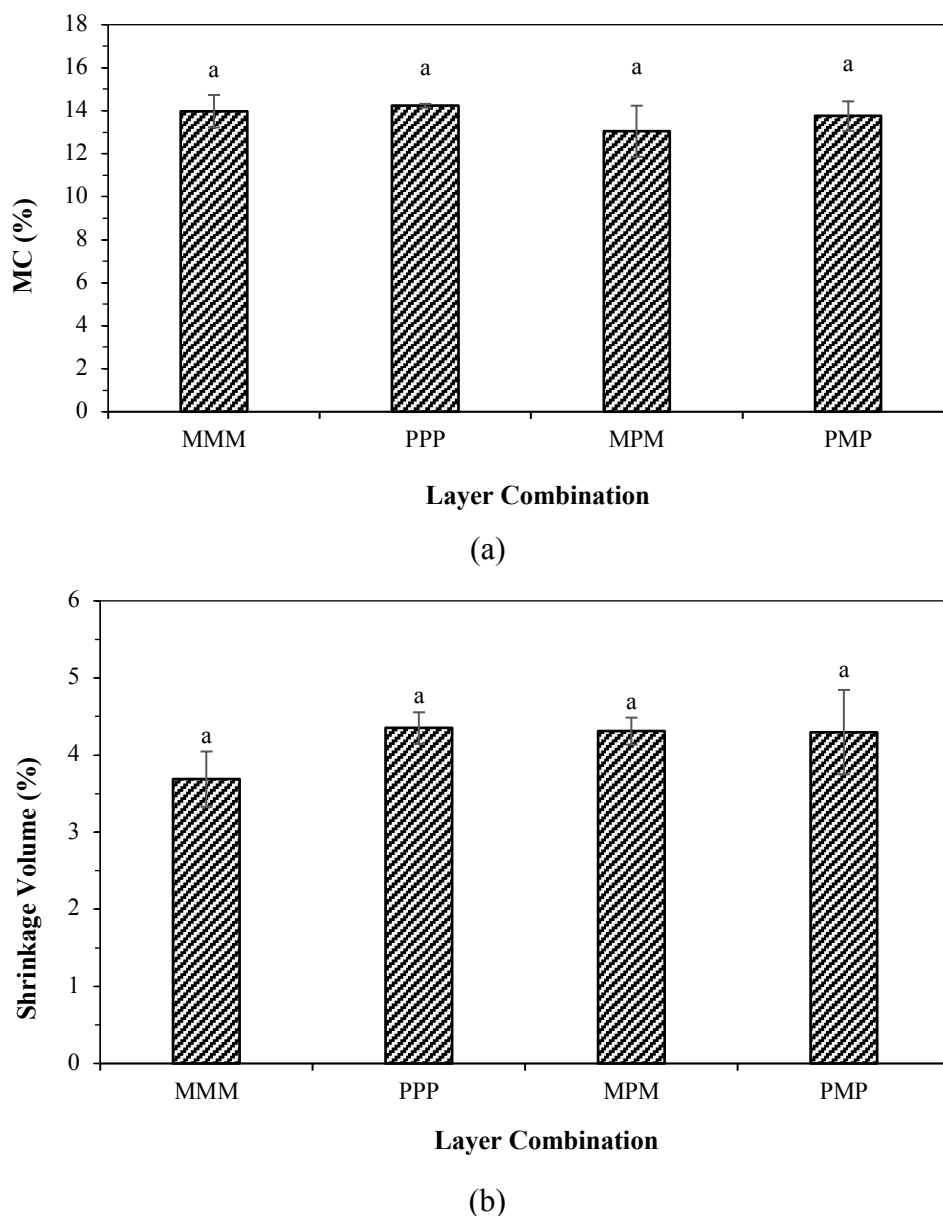
Fig. 11. (a) MC and (b) volume shrinkage of CLT in the variation of layer combination (layer combinations followed by different letters mean that they have significantly different values from the ANOVA results ($\alpha = 0.05$). Data is the mean value of n = 3).

Fig. 11 shows that the MC tends to be higher in the PPP CLT of 14.23% with a shrinkage of 4.35%, followed by the MMM CLT of 13.98% with a shrinkage of 3.69%, then PMP CLT of 13.75% with a shrinkage of 4.30%, and the smallest MPM CLT of 13.04% with a shrinkage of 4.31%. The higher PPP CLT shrinkage value than other samples is in line with the shrinkage characteristics of the raw materials in **Table 4**. Several others also showed the effect of moisture

content on the CLT dimensional study (Kukk et al. 2021; Pang and Jeong 2020). The higher value of CLT MC is more susceptible to dimensional changes affecting mechanical quality (Silva et al. 2016). However, the ANOVA results showed that the combination of CLT layers had no effect on MC and shrinkage. In addition, all samples could meet the requirements for the CLT JAS 3079 standard, which was < 15%. This means that there is no effect of differences in MC and environmental influences on shrinkage and other mechanical parameters of CLT. In addition to shrinkage, the CLT dimension parameters are WA and TS, shown in **Fig. 12**.
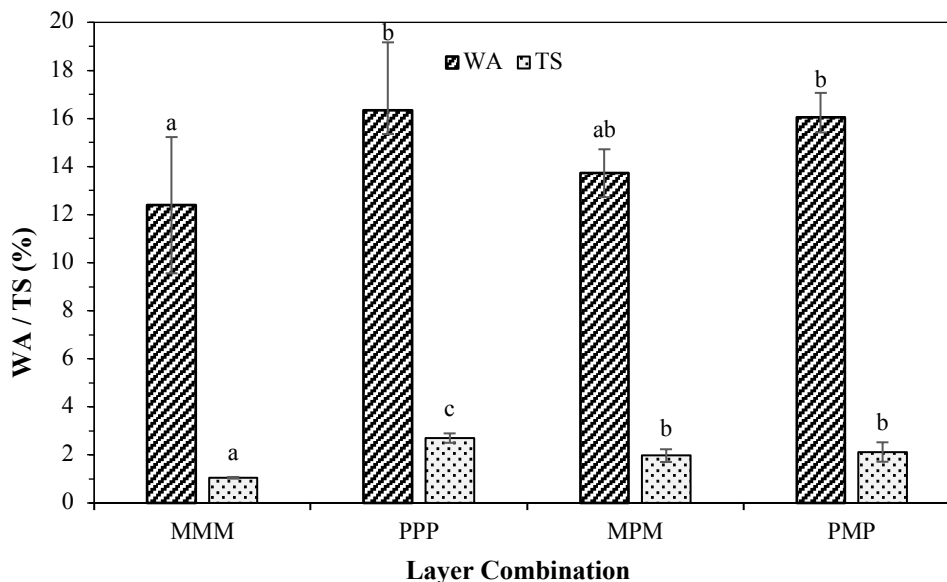
Fig. 12. Dimensional stability of CLT in the variation of layer combination (Graphs with the same color or bar pattern followed by different letters mean that they have significantly different values from the ANOVA results (α = 0.05). Data is the mean value of n = 3).

The graph in **Fig.12** shows the percentage of WA CLT positively correlates with TS in each sample. Respectively, the highest WA and TS values occurred in PPP CLT at 16.33% and 2.70%, followed by PMP CLT of 16.05% and 2.12%, then MPM CLT was 13.74% and 1.97%, and the smallest MMM CLT of 12.39% and 1.05%. The ANOVA results showed that the combination of layers significantly affected the dimensional stability of the CLT. DMRT proved a significant difference in dimensional stability between single and hybrid CLTs. The MMM CLT was significantly more dimensionally stable than the MPM CLT and PMP CLT, while the PPP CLT was the opposite. This is due to the higher weight of puspa wood SG than mangium. The research of Pang and Jeong (2020) also proved lower dimensional stability in CLT with high SG. The larger puspa cell wall provides more space for water to seep (Priadi et al. 2019; Rowell and Youngs 1981). This causes the TS vulnerability to PPP CLT to increase in bound water content. The combination of puspa CLT with mangium can reduce the impact of TS. A high percentage of TS in CLT with a combination of puspa can affect the WD and BD, as shown in **Fig. 13**.

The graph in **Fig. 13** shows the highest percentage of WD and BD occurred in PPP CLT at 61.01% and 78.61%, followed by PMP CLT of 39.54% and 49.86%; then MPM CLT was 34.85% and 38.86%; and the smallest MMM CLT was 31.12% and 34.59%. The ANOVA results showed a combination of layers that significantly affected the percentage of CLT WD and BD. DMRT proved a significant difference in delamination between PPP CLT and other samples. This shows the significant impact of TS PPP CLT on its vulnerability to WD and BD. However, a significant

decrease in the percentage of CLT delamination can occur by combining puspa and mangium wood. The percentage of delamination of MPM CLT and PMP CLT was not significantly different from that of MMM CLT. This shows that the delamination resistance of hybrid CLT is better than PPP CLT. However, all CLT samples did not meet the JAS 3079 standard with a delamination percentage of < 10%. The research of Muñoz et al. (2022) also reported that CLT from *Gmelina arborea* and *Tectona grandis* used EPI adhesive with a delamination percentage to the water of > 50% and did not meet the standard. This indicates the importance of coating or special treatment on the wood material to increase the dimensional stability of CLT. Based on the overall physical parameters, the combination of mangium and puspa CLT has better dimensional stability and delamination resistance than PPP CLT and higher density than MMM CLT.
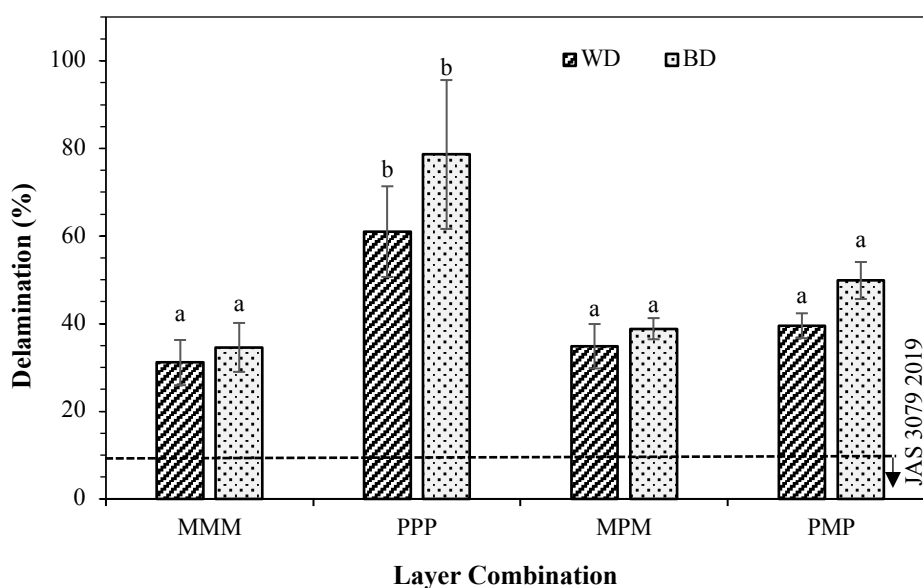
Fig. 13. Water and boiling delamination of CLT in the variation of layer combination (Graphs with the same color or bar pattern followed by different letters mean that they have significantly different values from the ANOVA results (α = 0.05). Data is the mean value of n = 3.).

3.3.2. Mechanical properties of CLT

CLT characterization was also carried out through mechanical parameters. The results showed that the mechanical strength tended to be different in each CLT sample. The mechanical MOE and MOR parameters of each CLT sample are shown in **Fig. 14**. The graphs in **Fig. 14** (a) show the stress-strain behavior of each CLT sample. The maximum load and deflection in each sample are calculated as MOE and MOR, shown in **Fig. 14** (b) and (c). The MOE value of CLT positively correlates with the MOR in each sample. The highest MOE and MOR values were found in PPP CLT at 10732 MPa and 39 MPa, followed by PMP CLT at 10724 MPa and 41 MPa, then MPM CLT at 10477 MPa and 33 MPa, and the smallest MMM CLT was 9461 MPa and 17 MPa. However, the ANOVA results showed no significant effect of the combination of CLT layers on the MOE value. This could be due to the similarity of the type of damage in the form of adhesive failure shown in **Fig. 15**. On the other hand, the graph in **Fig. 8** (b) shows the trend of storage modulus of PU 1.2, which is still increasing up to 200 minutes. Therefore, a longer CLT compression time is needed to improve the adhesive quality and produce a combination of mangium and puspa CLT with more optimal bending strength.

MMM CLT
y = 118.68x − 165.72
R² = 0.8998

PPP CLT
y = 139x − 661.91
R² = 0.9966

MPM CLT
y = 141.78x − 108.86
R² = 0.9412

PMP CLT
y = 136.13x − 582.96
R² = 0.9986
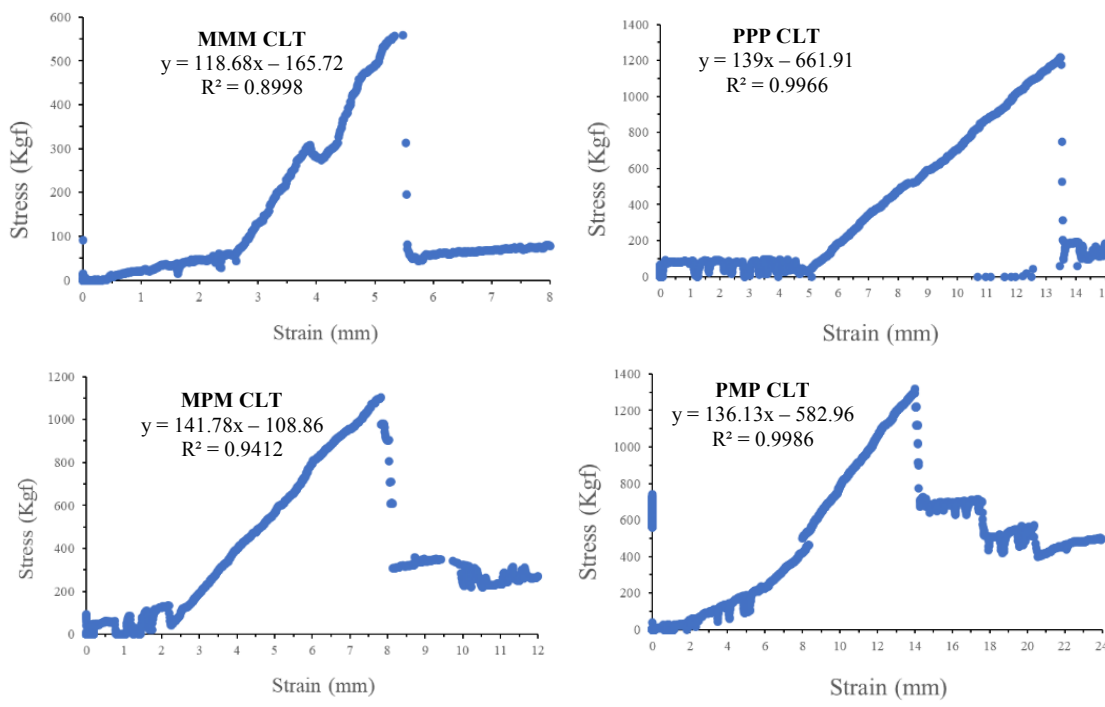
(a)
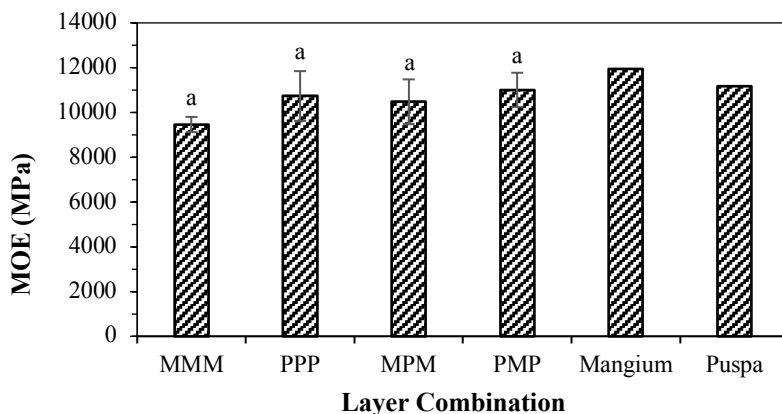
(b)
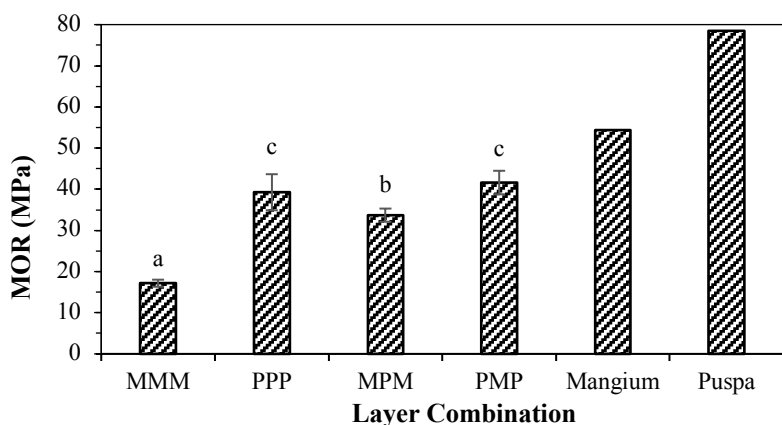
(c)

Fig. 14. Graph of (a) stress-strain bending along with the strength values of (b) MOE and (c) MOR (Graphs (b) and (c) with the same color or bar pattern followed by different letters mean that they have significantly different values from the ANOVA results (α = 0.05) and citing the solid wood bending strength of mangium (Komariah et al. 2015) and puspa (Mardikanto et al. 2017). Data is the mean value of n = 3).
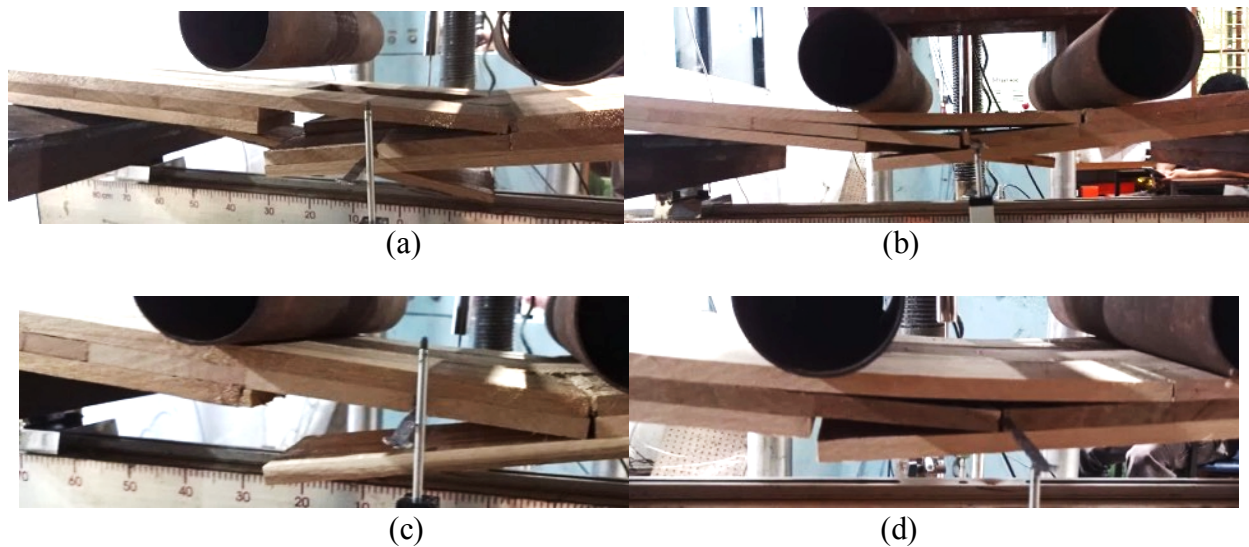
Fig. 15. Failure to bending test of (a) MMM, (b) PPP, (c) MPM, and (d) PMP CLT.

Although the MOE values of all CLT samples were not significantly different, the MOR parameters showed different results in **Fig. 14**. The ANOVA results showed a significant effect of layer combination on the CLT MOR value. DMRT proved a significant difference between MMM CLT and MPM CLT as well as with PPP CLT and PMP CLT. This shows a positive correlation between the density and MOR of CLT. Other studies also showed the same trend between the density and bending strength of CLT (Corpataux et al. 2020; Feng and Chiang 2020; Kim 2020). Panels with higher density will have the capability to withstand large amounts of stress, thereby reducing bending failure in the wood (Feng and Chiang 2020). However, the overall sample has lower bending strength than the solid wood in Figures 15 (e) and (f). This is due to the presence of adhesive joints in CLT, which have lower resistance than wood materials (Mardikanto et al. 2017). This indicates that the bending strength of the hybrid CLT is better than the MMM CLT. In addition to bending, all CLTs were tested for shear strength, as shown in **Fig. 16**.
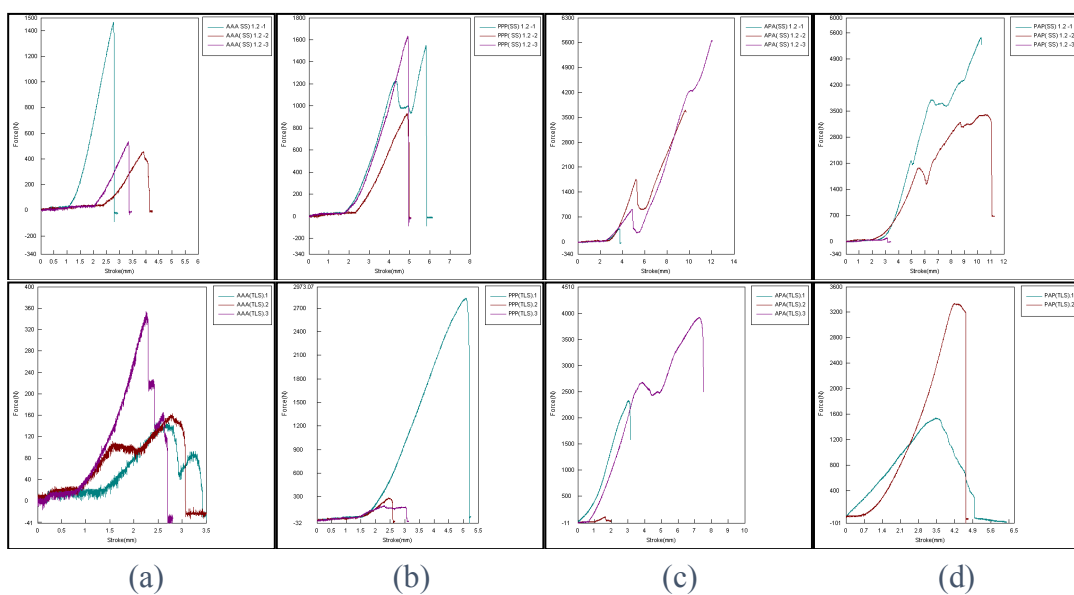
Fig. 16. The graphs of Shear stress-strain (top) parallel and (bottom) perpendicular to the grain (a) MMM CLT, (b) PPP CLT, (c) MPM CLT, and (d) PMP CLT.

The graphs in **Fig. 16** (a)-(d) show the stress-strain due to shear load for each CLT sample. It can be seen that there is a significant difference in the shear stress-strain graph between replicates, especially in the PPP CLT sample. This is due to the difference in the failure area shown in **Fig. 17**. Variations in failure due to shear tests were also experienced by other studies. The research of Yusof et al. (2019b) also tested the bending and shear strength of mangium CLT using PU adhesive and suffered various types of failure, including adhesive failure and wood failure. The surface roughness of puspa wood which tends to be lower than that of mangium in **Table 6,** can be a factor in the susceptibility of PPP CLT to adhesive failure. In addition, denser and harder wood will make it difficult for the substrate to bond to each other between surfaces (Hovanec 2015). Therefore, the combination of hybrid CLT promotes the stabilization of interactions between the surfaces so that MPM CLT and PMP CLT have less adhesive failure.

(a)   (b)   (c)   (d)
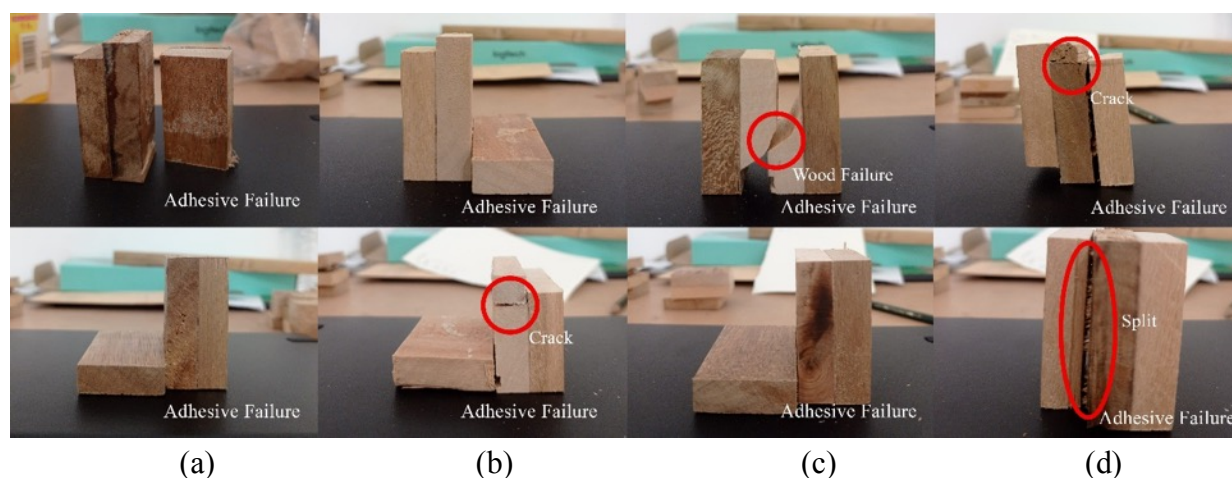
Fig. 17. Shear failure (top) parallel and (bottom) perpendicular to the grain of (a) MMM CLT,
(b) PPP CLT, (c) MPM CLT, and (d) PMP CLT.

Although the average shear strength of CLT in several combinations of layers is quite varied, the JAS 3079 standard provides a limit for shear strength for each sample. The standard states the success of shear strength in samples with a minimum wood percentage failure (WPF) of 90%. The shear strength and WPF of CLT are shown in **Table 7**.

Table 7. Shear strength of CLT in the variation of layer combinations

Layer Combination of CLT	Shear Strength (MPa)		WPF(%) $\geq$ 90%*	
	Parallel to Grain	Perpendicular to Grain	Parallel to Grain	Perpendicular to Grain
MMM	0.99 ± 1.01^a	0.11 ± 0.31^a	0.00	0.00
PPP	1.10 ± 0.31^a	0.54 ± 0.73^a	0.00	0.00
MPM	2.59 ± 2.14^a	1.29 ± 0.47^a	66.67	0.00
PMP	2.37 ± 2.12^a	1.73 ± 2.31^a	33.33	33.33

Notes: *According to JAS 3079 (Japanese Agricultural Standard 2019). Numbers in the same column followed by different letters mean that they have significantly different values from the ANOVA results ($\alpha = 0.05$). Data is the average value of n = 3.

The data in **Table 7** shows the shear strength of CLT in both grain directions, whose standard deviation is affected by the type of failure in **Fig. 17**. These data show the potential of hybrid CLT to withstand shear loads in both grain directions. Overall, all samples cannot meet the JAS 3079 standard. However, as many as two individual samples of PMP CLT could have WPF above the JAS 3079 standard in both grain directions, while MPM CLT was only in the direction parallel to

the grain. This shows the capability of the hybrid CLT combination to improve the quality of a single CLT in terms of mechanical strength. Based on the overall mechanical parameters, PMP CLT can have a bending quality that is not significantly different from PPP CLT and has a better shear quality than MPM CLT, MMM CLT, and PPP CLT.

4. Conclusions

This study revealed that the PU 1.2 adhesive could harden and reach the gelatinization point before the pressing time limit is 200 minutes at 25°C. This is evidenced by the gelatinization time of PU 1.2 from the reaction of isocyanate and polyol for 182.10 minutes at room temperature, the formation of urethane groups on PU 1.2 through FTIR and Py-GCMS analysis, as well as the ability to increase thermo-mechanically at low temperatures. However, the thermo-mechanical test showed the PU 1.2 storage modulus potential to increase the value above 200 minutes. The interaction of PU 1.2 on mangium and puspa wood as CLT material also showed a similar wettability behavior. Utilization of puspa wood in the form of single or hybrid CLT (PPP, PMP, MPM) can increase board density. However, the dimensional stability and delamination resistance of MMM CLT, MPM CLT, and PMP CLT are better than PPP CLT at the same moisture content and volume shrinkage conditions, but all samples do not meet the JAS 3079 (2019) standard. This shows that CLT's density and dimensional stability are better than that of a single CLT. In addition, the bending strength of PMP CLT can match PPP CLT. All shear test samples did not meet the JAS 3079 standard. Individually, as many as one sample of PMP CLT shear strength complied with the JAS 3079 standard in each grain direction. However, MPM CLT and single CLT were very susceptible to shear adhesive failure, especially in the direction of perpendicular to the grain. Therefore, the CLT hybrid of PMP can be further developed to increase its dimensional stability and mechanical strength.

Acknowledgments

References

Adnan, N. A., Md Tahir, P., Husain, H., Lee, S. H., Uyup, A. M. K., Arip, M. M. N., and Ashaari, Z. 2021. Effect of ACQ Treatment on Surface Quality and Bonding Performance of Four Malaysian Hardwoods and Cross Laminated Timber (CLT). *European Journal of Wood and Wood Products* 79(2): 285-299. DOI: 10.1007/s00107-020-01609-7

American National Standards Institute. 2018. *ANSI/APA PRG 320: Standard for Performance-Rated Cross Laminated Timber*. APA - The Engineered Wood Association, Washington, USA.

American Society for Testing Materials. 2014. *Annual Book of ASTM Standards D-143: Standard Test Methods for Small Clear Specimen of Wood*. American Society for Testing Materials, Pennsylvania, USA.

Aicher, S., Hirsch, M., and Christian, Z. 2016. Hybrid Cross-Laminated Timber Plates with Beech Wood Cross-Layers. *Construction and Building Materials* 124: 1007-1028. DOI: 10.1016/j.conbuildmat.2016.08.051

Aisyah, S., Haryadi, J., Maulana, M. I., Prasetia, D., Hidayat, W., Lubis, M. A. R., Kim, N. H. and Febrianto, F., 2021. Effects of Strands Pre-treatment and Adhesive Type on the Properties of Oriented Strand Board Made from Gmelina (*Gmelina arborea*) Wood. *Jurnal Sylva Lestari* 9(3): 475-487. DOI: 10.23960/jsl.v9i3.532

Amiri, A., Ottelin, J., Sorvari, J., and Junnila, S. 2020. Cities as Carbon Sinks-Classification of Wooden Buildings. *Environmental Research Letters* 15(9): 094076. DOI: 10.1088/1748-9326/aba134

Aristri, M. A., Lubis, M. A. R., Laksana, R. P. B., Falah, F., Fatriasari, W., Ismayati, M., Wulandari, A. P., Nurindah, and Ridho, M. R. 2021. Bio-Polyurethane Resins Derived from Liquid Fractions of Lignin for the Modification of Ramie Fibers. *Jurnal Sylva Lestari* 9(2): 223-238. DOI: 10.23960/jsl29223-238

Aristri, M. A., Lubis, M. A. R., Laksana, R. P. B., Sari, R. K., Iswanto, A. H., Kristak, L., Antov, P., and Pizzi, A. 2022. Thermal and Mechanical Performance of Ramie Fibers Modified with Polyurethane Resins Derived from *Acacia mangium* Bark Tannin. *Journal of Material Research and Technology* 18: 2413-2427. DOI:10.1016/j.jmrt.2022.03.131

Baskara, M. I. A., Hapsoro, D., Maulana, M. I., Prasetia, D., Hidayat, W., Lubis, M. A. R., Kim, N.H. and Febrianto, F., 2022. Physical and Mechanical Properties of Oriented Strand Board from Three Species of Plantation Forests at Various Resin Contents. *Jurnal Sylva Lestari* 10(1): 49-62. DOI: 10.23960/jsl.v10i1.519

Bekhta, P., Sedliaċik, J., and Bekhta, N. 2020. Effects of Selected Parameters on the Bonding Quality and Temperature Evolution Inside Plywood During Pressing. *Polymers* 12(5): 1035. DOI: 10.3390/polym12051035

Bossu, J., Beauchĕne, J., Estevez, Y., Duplais, C., and Clair, B. 2016. New Insights on Wood Dimensional Stability Influenced by Secondary Metabolites: The Case of A Fast-Growing Tropical Species *Bagassa guianensis* Aubl. *PLOS One* 11(3): e0150777. DOI: 10.1371/journal.pone.0150777

Corpataux, L., Okuda, S., and Kua, H. W. 2020. Panel and Plate Properties of Cross-Laminated Timber (CLT) with Tropical Fast-Growing Timber Species in Compliance with Eurocode 5. *Construction and Building Materials* 261: 119672. DOI: 10.1016/j.conbuildmat.2020.119672

Chen, N., Lin, Q., Zheng, P., Rao, J., Zeng, Q., and Sun, J. 2019. A Sustainable Bio-Based Adhesive Derived from Defatted Soy Flour and Epichlorohydrin. *Wood Science and Technology* 53(4): 801-817. DOI: 10.1007/s00226-019-01102-2

Darmawan, W., Nandika, D., Noviyanti, E., Alipraja, I., Lumongga, D., Gardner, D., and Gerardin, P. 2018. Wettability and Bonding Quality of Exterior Coatings on Jabon and Sengon Wood Surfaces. *Journal of Coatings Technology and Research* 15(1): 95-104. DOI: 10.1007/s11998-017-9954-1

Delpech, M. C., and Miranda, G. S. 2012. Waterborne Polyurethanes: Influence of Chain Extender in FTIR Spectra Profiles. *Central European Journal of Engineering* 2(2): 231-238. DOI: 10.2478/s13531-011-0060-3

Dyer, E., and Read, R. E. 1961. Thermal Degradation of O-1-Hexadecyl N-1-Naphthylcarbamates and Related Compounds. *Journal of Organic Chemistry* 26(11): 4388-4394. DOI: 10.1021/jo01069a050

Dyer, E., and Wright, G. C. 1959. Thermal Degradation of Alkyl N-Phenylcarbamates. *Journal of the American Chemical Society* 81(9): 2138-2143. DOI: 10.1021/ja01518a030

Feng, T. Y., and Chiang, L. K. 2020. Effects of Densification on Low-Density Plantation Species for Cross-Laminated Timber. *AIP Conference Proceedings* 2284(1). DOI: 10.1063/5.0029041

Follesa, M., Christovasilis, I. P., Vassallo, D., Fragiacomo, M., and Ceccotti, A. 2013. Seismic Design of Multi-Storey Cross Laminated Timber Buildings According to Eurocode 8. *Ingegneria Sismica* 30(4): 27-53.

Garcia-Pacios, V. G., Iwata, Y., Colera, M., and Martinez, J. M. M. 2011. Influence of The Solids Content on The Properties of Waterborne Polyurethane Dispersions Obtained with Polycarbonate of Hexanediol. *International Journal of Adhesion and Adhesives* 31: 787-794. DOI: 10.1016/j.ijadhadh.2011.05.010

Ghimire, P., Paudel, P., Bhatta, B., Gautam, P., and Devkota, N. 2020. Importance of Trees Outside Forest (TOF) for Immediate Earthquake Response. *Journal of Biodiversity Conservation and Bioresource Management* 6(1): 9-16.

Gurunathan, T., Mohanty, S., and Nayak, S. K. 2015. Isocyanate Terminated Castor Oil-Based Polyurethane Prepolymer: Synthesis and Characterization. *Progress in Organic Coatings* 80: 39-48. DOI: 10.1016/j.porgcoat.2014.11.017

Hadjib, N., Massijaya, M. Y., and Hadi, Y. S. 2010. Address Technical Gaps in Producing Bio-Composite Products: Identify Suitable Wood Species and Evaluate Mechanical Properties. *CFC/ITTO: Utilization Of Small Diameter Logs from Sustainable Sources for Bio-Composite Products*. Bogor: Institut Pertanian Bogor.

Hariz, T. M. R., Santosa, I. A., Maulana, M. I., Marwanto, M., Prasetia, D., Hidayat, W., Lubis, M. A. R., Kim, N. and Febrianto, F., 2021. Effects of Resin Content on the Characteristics of Bamboo Oriented Strand Board Prepared from Strands of Betung, Ampel, and Their Mixtures. *Jurnal Sylva Lestari 9*(3): 54-465. DOI: 10.23960/jsl.v9i3.520

Hass, P., Wittel, F. K., Mendoza, Herrmann, H. J., and Niemz, P. 2012. Adhesive Penetration in Beech Wood: Experiments. *Wood Science and Technology* 46: 243-256. DOI: 10.1007/s00226-011-0410-6

Hazmi, A. S. A., Aung, M. M., Abdullah, L. C., Salleh, M. Z., and Mahmood, M. H. 2013. Producing Jatropha Oil-Based Polyol via Epoxidation and Ring Opening. *Industrial Crops and Products* 50: 563-567. DOI: 10.1016/j.indcrop.2013.08.003

Himes, A., and Busby, G. 2020. Wood Buildings as A Climate Solution. *Developments in the Built Environment* 4: 100030. DOI: 10.1016/j.dibe.2020.100030

Hovanec, D. 2015. Effect of Wood Characteristics on Adhesive Bond Quality of Yellow-Poplar for Use in Cross-Laminated Timbers [graduate thesis]. West Virginia University, West Virginia, USA.

Hummel, J., and Seim, W. 2019. Displacement-Based Design Approach to Evaluate The Behaviour Factor for Multi-Storey CLT Buildings. *Engineering Structures* 201: 109711. DOI: 10.1016/j.engstruct.2019.109711

International Organization for Standardization. 1997. *Geometrical Product Specifications (GPS) Surface texture: Profile Method. Terms, Definitions and Surface Texture Parameters*. ISO 4287-1977. International Organization for Standardization, Geneva, Switzerland.

Jankowska, A., Boruszewski, P., Drozdzek, M., Rebkowski, B., Kaczmarczyk, A., and Skowronska, A. 2017. The Role of Extractive and Wood Anatomy in The Wettability and Free Surface Energy of Hardwoods. *BioResources* 13(2): 3082-3097. DOI: 10.15376/biores.13.2.3082-3097

Japanese Agricultural Standard. 2019. *JAS 3079: Cross Laminated Timber*. Ministry of Agriculture, Forestry, and Fisheries, Tokyo, Japan.

Karacebeyli, E., and Douglas, B. 2013. *CLT Handbook: Cross Laminated Timber*. FPInnovations and Binational Softwood Lumber Council, Quebec, Canada.

Karlinasari, L., Fredisa, Y., Adzkia, U., Fauziyyah, S., Dwiyanti, F. G., and Siregar, I. Z. 2021. Use of a Pin-Penetration Wood Density Meter to Determine the Density of 25 Indonesian Species. *BioResources* 16(2): 3032-3045. DOI: 10.15376/biores.16.2.3032-3045

Karlinasari, L., Lestari, A. T., and Priadi, T. 2018. Evaluation of Surface Roughness and Wettability of Heat-Treated, Fast-Growing Tropical Wood Species Sengon (*Paraserianthes*

falcataria (L.) I.C.Nielsen), Jabon (*Anthocephalus cadamba* (Roxb.) Miq), and Acacia (*Acacia mangium* Willd.). *International Wood Products Journal* 9(4): 1-7. DOI: 10.1080/20426445.2018.1516918

Kim, K. H. 2020. Influence of Layer Arrangement on Bonding and Bending Performances of Cross-Laminated Timber using Two Different Species. *BioResources* 15(3): 5328-5341. DOI: 10.15376/biores.15.3.5328-5341

Komariah, R. N., Hadi, Y. S., Massijaya, M. Y., and Suryana, J. 2015. Physical-Mechanical Properties of Glued Laminated Timber Made from Tropical Small-Diameter Logs Grown in Indonesia. *Journal of the Korean Wood Science and Technology* 43(2): 156-167. DOI: 10.5658/wood.2015.43.2.156

Kong, X., Liu, G., and Curtis, J. M. 2011. Characterization of Canola Oil Based Polyurethane Wood Adhesives. *International Journal of Adhesion and Adhesives* 31(6): 559-564. DOI: 10.1016/j.ijadhadh.2011.05.004

Kuilen, J. W. G., Ceccotti, A., Xia, Z., and He, M.. 2011. Very Tall Wooden Buildings with Cross Laminated Timber. *Procedia Engineering* 14: 1621-1628. DOI: 10.1016/j.proeng.2011.07.204

Kukk, V., Bella, A., Kers, J., and Kalamees, T. 2021. Airtightness of Cross-Laminated Timber Envelopes: Influence of Moisture Content, Indoor Humidity, Orientation, and Assembly. *Journal of Building Engineering* 44: 102610. DOI: 10.1016/j.jobe.2021.102610

Lai, Y., Qian, Y., Yang, D., Qiu, X., and Zhou, M. 2021. Preparation and Performance of Lignin-Based Waterborne Polyurethane Emulsion. *Industrial Crops and Products* 170: 113739. DOI: 10.1016/j.indcrop.2021.113739

Liang, X., Sun, X., Lu, Q., Ren, L., Liu, M., Su, Y., Wang, S., Lu, H., Gao, B., Zhao, W., Sun, J., Gao, Z., and Chen, L. 2021. VOC Emission Inventory of Architectural Coatings and Adhesives for New Buildings in China Based on Investigated and Measured Data. *Atmospheric Environment* 245: 118014. DOI: 10.1016/j.atmosenv.2020.118014

Liao, Y., Tu, D., Zhou, J., Zhou, H., Yun, H., Gu, J., and Hu, C. 2017. Feasibility of Manufacturing Cross-Laminated Timber using Fast-Grown Small Diameter Eucalyptus Lumbers. *Construction and Building Materials* 132: 508-515. DOI: 10.1016/j.conbuildmat.2016.12.027

Liu, Y., Liang, H., Li, S., Liu, D., Long, Y., Liang, G., and Zhu, F. 2019. Preparation of Waterborne Polyurethane with High Solid Content and Elasticity. *Journal of Polymer Research* 26(146): 1-8. DOI: 10.1007/s10965-019-1795-4

Lokmal, N., and Noor, M. A. G. 2010. Variation of Specific Gravity in *Acacia mangium*. *Journal of Agrobiotechnology* 70(1): 69-88.

Lubis, M. A. R., Handika, S. O., Sari, R. K, Iswanto, A. H., Antov, P., Kristak, L., Lee, S. H., and Pizzi, A. 2022. Modification of Ramie Fiber via Impregnation with Low Viscosity Bio-Polyurethane Resins Derived from Lignin. *Polymers (Basel)*. 14 (11): 2165. DOI: 10.3390/polym14112165

Mallo, M. F. L., and Espinoza, O. 2014. Outlook for Cross-Laminated Timber in The United States. *BioResources* 9(4): 7427-7443. DOI: 10.15376/biores.9.4.7427-7443

Mardikanto, T., Karlinasari, L., and Bahtiar, E. T. 2017. *Sifat Mekanis Kayu*. Bogor: IPB Press.

Marko, G., Bejo, L., and Takats, P. 2016. Cross-laminated timber made of Hungarian raw materials. *IOP Conference Series: Materials Science and Engineering* 123: 012059. DOI: 10.1088/1757-899x/123/1/012059

Menard, K. P. 2008. *Dynamic Mechanical Analysis: A Practical Introduction*. CRC Press, New York, USA.

Moslemi, A., Koohi, M. Z., Behzad, T., and Pizzi, A. 2020. Addition of Cellulose Nanofibers Extracted from Rice Straw to Urea Formaldehyde Resin; Effect on The Adhesive Characteristics and Medium-density Fiberboard Properties. *International Journal of Adhesion and Adhesives* 99: 102582. DOI: 10.1016/j.ijadhadh.2020.102582

Muñoz, F., Tenorio, C., Moya, R., and Mora, A. N. 2022. CLT Fabricated with *Gmelina arborea* and *Tectona grandis* Wood from Fast-Growth Forest Plantations: Physical and Mechanical Properties. *Journal of Renewable Materials* 10(1): 1-17. DOI: 10.32604/jrm.2022.017392

Nacas, A. M., Ito, N. M., Sousa Jr, R. R. D., Spinacė, M. A., and Santos, D. J. D. 2017. Effects of NCO:OH Ratio on The Mechanical Properties and Chemical Structure of Kraft Lignin-Based Polyurethane Adhesive. *Journal of Adhesion* 93(1-2): 18-29. DOI: 10.1080/00218464.2016.1177793

Naresh, K., Shankar, K., and Velmurugan, R. 2018. Digital Image Processing and Thermo-Mechanical Response of Neat Epoxy and Different Laminate Orientations of Fiber Reinforced Polymer Composites for Vibration Isolation Applications. *International Journal of Polymer and Characterization* 23(8): 684-709. DOI: 10.1080/1023666x.2018.1494431

Nepal, P., Skog, K. E., McKeever, D. B., Bergman, R. D., Abt, K. L., and Abt, R. C. 2016. Carbon Mitigation Impacts of Increased Softwood Lumber and Structural Panel use for Nonresidential Construction in The United States. *Forest Products Journal* 66(1-2): 77-87. DOI: 10.13073/fpj-d-15-00019

Neykov, N., Antov, P., and Savov, V. 2020. *Circular Economy Opportunities for Economic Efficiency Improvement in Wood-Based Panel Industry*. Conference: 11th International Scientific Conference "Business and Management 2020". Vilnius, Lithuania. DOI: 10.3846/bm.2020.493

Nugroho, W. D., Marsoem, S. N., Yasue, K., Fujiwara, T., Nakajima, T., Hayakawa, M., Nakaba, S., Yamagishi, Y., Jin, H. O., Kubo, T., and Funada, R. 2012. Radial Variations in The Anatomical Characteristics and Density of The Wood of *Acacia mangium* of Five Different Provenances in Indonesia. *Journal of Wood Science* 58: 185-194. DOI: 10.1007/s10086-011-1236-4

Nussbaum, R. M., Sterley, M. 2002. The Effect of Extractive Content on Glue Adhesion and Surface Wettability of Wood. *Wood Fiber and Science* 34(1): 57-71.

Oliviero, M., Stanzione, M., D'Auria, M., Sorrentino, L., Iannace, S., and Verdolotti, L. 2019. Vegetable Tannin as A Sustainable UV Stabilizer for Polyurethane Foams. *Polymers (Basel)* 11(3): 1-16. DOI: 10.3390/polym11030480

Pajchrowski. G., Andrzej, N., Lewandowska, A., and Strykowski, W. 2014. Wood as A Building Material in The Light of Environmental Assessment of Full Life Cycle of Four Buildings. *Construction and Building Materials* 52: 428-436. DOI: 10.1016/j.conbuildmat.2013.11.066

Pang, S. J., and Jeong, G. Y. 2020. Swelling and Shrinkage Behaviors of Cross-Laminated Timber Made of Different Species with Various Lamina Thickness and Combinations. *Construction and Building Materials* 240: 117924. DOI: 10.1016/j.conbuildmat.2019.117924

Poh, A. K., Sin, L. C., Foon, C. S., and Hock, C. C. 2014. Polyurethane Wood Adhesive from Palm Oil-Based Polyester Polyol. *Journal of Adhesion Science and Technology* 28(11): 1020-1033. DOI: 10.1080/01694243.2014.883772

Priadi, T., Sholihah, M., and Karlinasari, L. 2019. Water Absorption and Dimensional Stability of Heat-Treated Fast-Growing Hardwoods. *Journal of the Korean Wood Science and Technology* 47(5): 567-578. DOI: 10.5658/wood.2019.47.5.567

Radabutra, S., Khemthong, P., Saengsuwan, S., Sangya, S. 2019. Preparation and Characterization of Natural Rubber Bio-Based Wood Adhesive: Effect of Total Solid Content, Viscosity, and Storage Time. *Polymer Bulletin* 77(12): 2737-2747. DOI: 10.1007/s00289-019-02881-1

Ravi-Sankar, M., Jain, V. K., Ramkumar, J., and Joshi, Y. M. 2011. Rheological Characterization of Styrene-Butadiene Based Medium and Its Finishing Performance using Rotational Abrasive Flow Finishing Process. *International Journal of Machine Tools and Manufacture* 51(12): 947-957. DOI: 10.1016/j.ijmachtools.2011.08.012

Rowell, R. M., and Youngs, R. L. 1981. *Dimensional Stabilization of Wood in Use*. Forest Product Lab Madison, Wisconsin, USA.

Schmid, J. 2019. Structural Fire Design-Statement on The Design of Cross-Laminated Timber (CLT). *Civil Engineering Research Journal* 7(5): 555721. DOI: 10.19080/cerj.2019.07.555721

Shi, S. Q., and Gardner, D. J. 2001. Dynamic Adhesive Wettability of Wood. *Wood and Fiber Science* 33(1): 58-68.

Silva, C., Branco, J. M., Ringhofer, A., Lourenço, P. B., and Schickofer, G. 2016. The Influences of Moisture Content Variation, Number and Width of Gaps on The Withdrawal Resistance of Self Tapping Screws Inserted in Cross Laminated Timber. *Construction and Building Materials* 125: 1205-1215. DOI: 10.1016/j.conbuildmat.2016.09.008

Statistics Indonesia. 2021. *Statistic of Forestry Production 2020*. Statistic Indonesia, Jakarta, Indonesia.

Sunija, A. J., Ilango, S. S., and Kumar, K. P. V. 2014. Synthesis and Characterization of Bio-Based Polyurethane from Benzoylated Cashewnut Husk Tannins. *Bulletin of Materials Science* 37(3): 735-741. DOI: 10.1007/s12034-014-0665-2

Szycher, M. 2012. *Szycher's Handbook of Polyurethanes*. CRC Press, New York, USA.

TAPPI (Technical Association of Pulp and Paper Industry). 1993. *Standard Method TAPPI T212 OM-18: One Percent Sodium Hydroxide Solubility of Wood and Pulp*. TAPPI, Atlanta, USA.

TAPPI (Technical Association of Pulp and Paper Industry). 2007. *Standard Method T207 CM-08: Water Solubility of Wood and Pulp*. TAPPI, Atlanta, USA.

Thébault, M., Pizzi, A., Essawy, H. A., Barhoum, A., and Van Assche, G. 2015. Isocyanate Free Condensed Tannin-Based Polyurethanes. *European Polymer Journal* 67: 513-526. DOI: 10.1016/j.eurpolymj.2014.10.022

Trutalli, D., and Pozza, L. 2018. Seismic Design of Floor–Wall Joints of Multi-Storey CLT Buildings to Comply with Regularity in Elevation. *Bulletin of Earthquake Engineering* 16(1): 183-201. DOI: 10.1007/s10518-017-0193-8

UNECE. 2021. *Annual Market Review 2010-2021 - Forest Products*. United Nations Publication, Geneva, Switzerland.

Wang, Z., Fu, H., Gong, M., Luo, J., Dong, W., Wang, T., and Chui, Y. H. 2017. Planar shear and bending properties of hybrid CLT fabricated with lumber and LVL. *Construction and Building Materials* 151: 172-177. DOI: 10.1016/j.conbuildmat.2017.04.205

Wimmers, G. 2017. Wood: A Construction Material for Tall Buildings. *Nature Reviews Materials* 2: 1-3. DOI: 10.1038/natrevmats.2017.51

Yusof, N., Md Tahir, P., Lee, S. H., Khan, M. A., and James, M. S. R. 2019a. Mechanical and Physical Properties of Cross-Laminated Timber Made from *Acacia mangium* Wood As Function of Adhesive Types. *Journal of Wood Science* 65(1): 1-11. DOI: 10.1186/s10086-019-1799-z

Yusof, N., Md Tahir, P., Muhammad Roseley, A. S., Lee, S. H., Halip, A. J., James, M. S. R, and Ashaari, Z. 2019b. Bond Integrity of Cross Laminated Timber from *Acacia mangium* Wood as Affected by Adhesive Types, Pressing Pressures and Loading Direction. *International Journal of Adhesion and Adhesives* 94: 24-28. DOI: 10.1016/j.ijadhadh.2019.05.010

Yusoh, A. S., Md Tahir, P., Uyup, A. M. K., Lee, S. H., Husain, H., and Khaidzir, M. O. 2021. Effect of Wood Species, Clamping Pressure and Glue Spread Rate on The Bonding Properties of Cross-Laminated Timber (CLT) Manufactured from Tropical Hardwoods. *Construction and Building Materials* 273(1): 121721. DOI: 10.1016/j.conbuildmat.2020.121721

Zelinka, S. L., Sullivan, K., Pei, S., Ottum, N., Bechle, N. J., Rammer, D. R., and Hasburgh, L. E. 2019. Small Scale Tests on The Performance of Adhesives Used in Cross Laminated Timber (CLT) at Elevated Temperatures. *International Journal of Adhesion and Adhesives* 95: 102436. DOI: 10.1016/j.ijadhadh.2019.102436

Zhang, Y., Xia, Z., Huang, H., and Chen, H. 2009. A Degradation Study of Waterborne Polyurethane Based on TDI. *Polymer Testing* 28(3): 264-269. DOI: 10.1016/j.polymertesting.2008.12.011

Zhou, J., Chui, Y. H., Niederwestberg, J., and Gong, M. 2020. Effective Bending and Shear Stiffness of Cross-Laminated Timber by Modal Testing: Method Development and Application. *Composites Part B: Engineering* 198: 108225. DOI: 10.1016/j.compositesb.2020.108225